metals

MDPI

Review

Research Progress on Corrosion Behaviors and Improvement Methods of Medical Degradable Mg−Based Alloys

Yuan Zhang [1,2], Wei Liu [1], Yun Liu [1,2,*], Mingshan Zhang [1], Yaqiang Tian [1,2] and Liansheng Chen [1]

[1] Key Laboratory of the Ministry of Education for Modern Metallurgy Technology, North China University of Science and Technology, Tangshan 063210, China
[2] School of Metallurgy and Energy, North China University of Science and Technology, Tangshan 063210, China
* Correspondence: liuyun@ncst.edu.cn; Tel.: +86-0315-8805420

Abstract: Due to the spontaneous degradability, excellent biocompatibility, favorable bone−inducibility, and antimicrobial properties, Mg−based alloys acting as miniature intravascular stents and bone−fixation materials have shown great development−potential. Regrettably, the uneven degradation model and excessive dissolution rate restricted their clinical application. In this study, the latest research on five methods (high−purity or amorphous, micro−alloying, heat−treatment, plastic−deformation, and surface modification) in medical Mg alloy degradation behaviors was reviewed. The corrosion mechanisms of Mg alloys under different processes were summarized. In addition, the effects of microstructure characteristics and film−layer features on corrosion resistance were systematically discussed. Ultimately, existing problems and future development directions of medical Mg−based alloys were reviewed.

Keywords: corrosion behavior; microstructure; high−purity; heat−treatment; surface modification; plastic−deformation; Mg−based alloys

Citation: Zhang, Y.; Liu, W.; Liu, Y.; Zhang, M.; Tian, Y.; Chen, L. Research Progress on Corrosion Behaviors and Improvement Methods of Medical Degradable Mg−Based Alloys. *Metals* **2023**, *13*, 71. https://doi.org/10.3390/met13010071

Academic Editor: Eric Hug

Received: 25 November 2022
Revised: 19 December 2022
Accepted: 19 December 2022
Published: 27 December 2022

1. Introduction

Traditional biomedical metallics (BMs) are commonly composed of permanent titanium, cobalt, stainless steel, etc. [1,2]. Long−term service has problems such as the release of toxic ions and acidic degradation products, which lead to tissue separation and even induced inflammation to aggravate the patient's condition [3–5]. Until now, medical implants with a Mg−matrix have possessed excellent loading−conductivity, spontaneous degradability in vivo, and good osteogenic and antibacterial functions, and can avoid the hidden dangers of secondary surgery and play a crucial role in human metabolism [6,7]. Detailed applications are shown in Figure 1 [8–10]. Unfortunately, Mg−based implants are prone to failure in a corrosive environment, especially in complex cyclic−stress, fatigue, and dynamic−flow conditions [11,12]. As a result, determining how to improve and enhance the corrosion resistance and explore the corrosion mechanism of medical Mg has become an urgent issue.

More importantly, excellent corrosion resistance is a prerequisite condition and necessary guarantee for medical Mg−implants. Furthermore, the property requirements of different parts varied for different Mg−based implants, which could cause failure during service. For instance, the implantation behavior of the WE43 bone screw in a dog−bone was studied by Byun et al. [13]. Results revealed that hydrogen was generated 3 weeks'−after implantation, and inflammation occurred 12 weeks'−after implantation. This was primarily due to the reaction of elements in the human body with Mg to produce bubbles, resulting in local alkaline effects. Similarly, Tie et al. [14] evaluated the degradation behavior of ZJ41 ureteral stents implanted in pigs. The results indicated that the corrosion rates of alloys decreased to 0.31 mm/y on the 14th day, which was caused by the gradual thickening of the corrosion layer and the obstruction of electron−transfer. Although the shape remained intact for 7 weeks following'−implantation, the corrosion rates gradually

increased. Elkamel et al. [15] investigated the electrochemical corrosion behaviors of the AZ91E magnesium alloy in a peritoneal aqueous solution. The results suggested that the corrosion current density of the alloys was 15.837 $\mu A \cdot cm^{-2}$ after 20 days of'−immersion. The value of H_2 evolution rates was very high, and could not meet the requirements of gastric implantation. Thus, new challenges were posed to research the preparation and improvement technologies for uncontrollable degradation behaviors of implanted alloys. In previous studies [16–23], authors found that the micro−alloying addition and plastic deformation optimized the degradation behavior of Mg−based alloys by refining the internal structure and stabilizing physical barrier coatings to improve corrosion resistance.

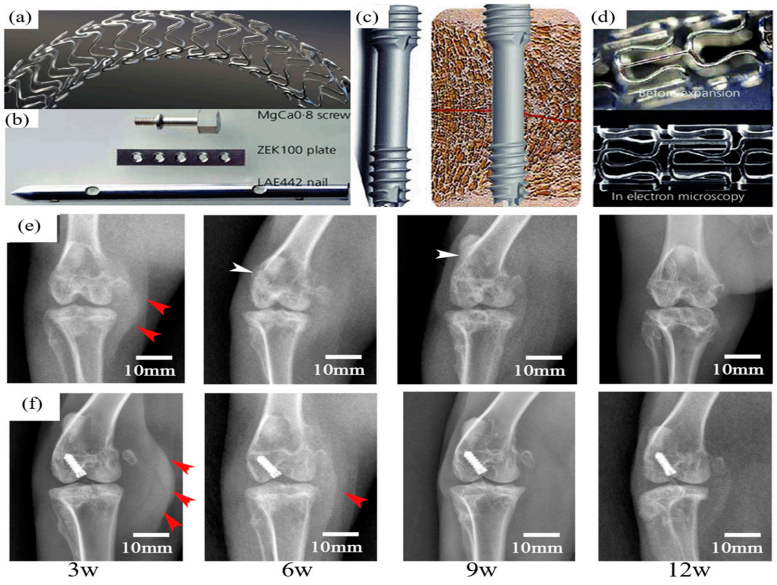

Figure 1. Real applications of biodegradable magnesium implants: (**a**,**d**) cardiovascular stents, (**b**) screws for orthopedic fixation, and (**c**) biodegradable orthopedic implants [8,9]; images of the rabbit knee joint in the anterior−posterior position at 3, 6, 9, and 12 weeks post−operation in (**e**) HP Mg group and (**f**) Ti group (red and white arrowheads indicate soft tissue swelling and periosteal reaction, respectively) [10]. Reprinted with permission from refs. [8–10]. Copyright 2022 Elsevier.

As a result, based on different improvement methods such as high−purity/amorphous, micro−alloying, heat treatment, plastic−deformation, and surface protective coatings, the latest research progress of medical Mg−based alloys was reviewed. Moreover, the corrosion mechanism of Mg alloys under various processes was summarized. Finally, existing problems and future development directions of medical Mg alloys were reviewed.

2. High−Purity and Amorphous

2.1. High−Purity Mg Alloys

Due to the remarkable difference in Volta potentials, it is prone to forming galvanic−corrosion in the matrix, especially for impurities, i.e., Cu, Fe, and Ni. Recently, with the booming development of metallic melting and metallic purification, the high−purity preparation of Mg alloys to improve corrosion resistance has become an important method. For instance, Woo et al. [24] investigated the effect of processing history on the corrosion behaviors of pure−Mg in a 3.5 wt% NaCl solution. The results revealed that the corrosion resistance of as−cast/as−extruded high−purity Mg showed significant differences despite having the same Fe contents (0.430 and 9.120 mm/y). They determined that the impurity of Fe and Si was precipitated into the Fe−Si phase by heat treatment prior to extrusion, leading to severe micro−galvanic corrosion. As a result, the control of the tolerance limit considering not only the impurity contents but also the processing history was required in designing alloys. Gao et al. [25] comparatively investigated the degradation behaviors of high−purity Mg under stress in Hanks' solution and in the

subcutaneous environment of rats. The results declared that when quantitative stress was applied, the corrosion rates of HP−Mg in Hanks' solution increased while the corrosion rates in the subcutaneous environment were not obviously different. The reason was that the stress could produce particle degradation products that attached to the surface differently and unevenly, whereas the fibrotic capsule suppressed the effects of stress in vivo by protecting the corrosion surfaces. Similarly, Ma et al. [26] studied the corrosion behavior of pure−Mg in rabbit bone. The results showed that the corrosion resistance of pure Mg first decreased and then increased as the implantation time extended. This was due to the corrosion product film that formed on the implanted pure−Mg screw, which mainly consisted of $Mg(OH)_2$, and the low contents of other impurities. Moreover, the long−term degradation evolution of high−purity Mg screw in vivo was evaluated by Yu [27]. They observed the alloy's own uniform degradation morphology and slow corrosion rates. They were attributed to the formation of $Mg(OH)_2$ and other hydroxyapatite products during the corrosion process, which had a barrier effect on dissolution behavior. Moreover, the good bone repair ability and long−term local/systemic biosafety granted it very high application prospects in the medical field.

2.2. Amorphous Mg Alloys

Fortunately, acting as medical metals, amorphous Mg alloys have excellent corrosion resistance with no grain boundaries, precipitation, or surface active−points such as inclusions and dislocations. Chen et al. [28] observed the amorphous $Mg_{67}Zn_8Ca_5$ alloy in simulated body fluid to display its own excellent corrosion resistance along with uniform degradation morphology. Furthermore, the degradation rates were linear in relation to the crystallization volume fraction. Moreover, Wang et al. [29] prepared the high−performance amorphous Mg−Zn−Ca through laser powder bed fusion, as shown in Figure 2, with a corrosion rate of 0.35 mm/y, which was within the ideal range of corrosion rates for human bone implants. The formation of dense and uniform products of $Ca_3(PO_4)_2$ and ZnO was beneficial to protect further corrosion and reduce the degradation rate of amorphous alloys. Zai et al. [30] studied the corrosion behaviors of metallic glass formed by adding Ga to a Mg−Zn−Ca block. The result indicated that as the Ga content increased, the corrosion current densities of the Mg−Zn−Ca−Ga metallic glass decreased significantly. This was because the addition of Ga to amorphous Mg was beneficial for forming dense degradation products and decreasing the pitting corrosion. Thus, the metallic glass showed a uniform corrosion morphology. Moreover, Li et al. [31] studied the corrosion behavior of metallic glasses consisting of $Mg_{66}Zn_{30}Ca_4$ with various particle sizes. The results showed that the corrosion resistance of a large−sized alloy is better, and therefore it can be used as a candidate material.

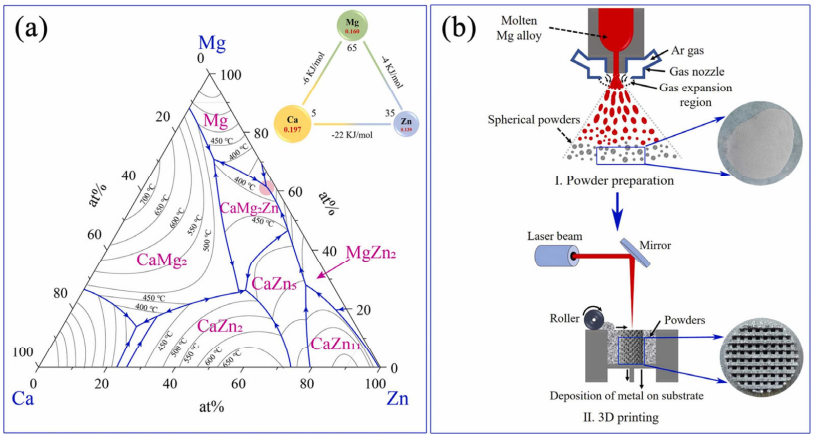

Figure 2. The compositions of the alloy selected in the present investigation are shown in (**a**) schematic diagram (**b**) of powder preparation and LPBF [29]. Reprinted with permission from ref. [29]. Copyright 2022 Elsevier.

3. Micro−Alloying

Due to the substandard mechanical strength and corrosion resistance of pure Mg, it is necessary to add some solute−elements. It can not only modify the distribution characteristics but also optimize the Volta potentials of the precipitates, which was beneficial to inhibit the intense galvanic−corrosion. Based on the elements'−properties, they can be roughly divided into three categories.

3.1. Nutrient Elements

Ca, Zn, Sr, and Mn are the essential trace elements for the human body, with no toxicity, which can promote enzyme synthesis and bone differentiation. As a result, they were usually used to improve the corrosion resistance of degradable Mg alloys. For instance, Makkar et al. [32] analyzed the in vitro degradation of binary as−cast Mg−xCa alloys (x = 0.5 or 5.0 wt.%) in a PBS solution. The dissolution rates of the Mg−Ca alloys increased notably with increasing Ca content. The poor corrosion resistance was associated with the presence of excessive intermetallic Mg_2Ca phases in the vicinity of the primary α−Mg phase. Due to the negative Volta potentials, Mg_2Ca was corroded more readily than α−Mg, which might expose the surface area to react with the PBS solution. In addition, 4 weeks'−after implantation, Mg−0.5Ca showed better biocompatibility and new bone formation ability. Subsequently, Chen et al. [33] studied the stress−corrosion behavior of novel Mg−Ca−La for guided bone regeneration. The results revealed that the bent Mg−0.2Ca−0.2La has a low corrosion rate (0.09 mm/y) and presents a uniform corrosion morphology (Figure 3a). It precipitated the $Mg_{12}La$/Mg_2Ca equiaxed crystals with Ca addition, creating more stable and uniform product layers.

Hu et al. [34] explored the corrosion behaviors of Mg alloys with various Zn contents (10, 20, 30, wt.%). They found that the corrosion current density decreased from 2.325×10^{-5} to 1.087×10^{-5} A/cm^2 as the Zn contents increased. The reason could be expressed from two perspectives: (i) As the Zn contents increased, the self−corrosion potentials of α−Mg increased; (ii) due to the difference in melting points (Mg/Zn), the low melting Zn was easily melted, covering the surface and delaying the breakdown of the protective film and improving the stability of the degradation layer. Abdel−Gawad et al. [35] further studied the corrosion behavior of Mg−xZn−yCa (x = 1, 2, 2.5 wt.%; y = 0.6, 0.6, 1.5 wt.%) in simulated body fluid, with the corrosion rates of 0.073, 0.043, and 0.280 mm/y, respectively. Moreover, the passivation region observed in the alloy indicated the formation of an HA layer. However, the addition of a large amount of Zn (2.5 wt.%) and Ca (more than 0.6 wt.%) can cause a fast corrosion rate due to the intense galvanic−corrosion.

Sr is an important component in human−bone and can promote bone growth and differentiation. Initially, Pan et al. [36] investigated the corrosion behaviors of Mg−1Zn−1Mn−xSr (x = 0, 0.5, 1.0, 1.5, 3.0) in Hanks' solution, with the rates of 0.051, 0.115, 0.149, 0.230, and 1.006 mm/y, respectively. They indicated that the corrosion rates increased linearly with increasing Sr contents due to the enhanced micro−galvanic corrosion. However, undermining $Mg_{17}Sr_2$ and α−Mg results in a dramatic increase in corrosion rates at a high Sr content (3.0 wt.%), resulting in high weight loss. Nevertheless, the alloys with Sr addition increased the corrosion area and decreased the maximum corrosion depths, leading to a more homogeneous corrosion morphology. Afterward, Wen et al. [37] explored the improvement in the in vitro and in vivo corrosion resistance of the Mg−1Zn−1Sn alloy by microalloying it with Sr. The corrosion morphology of Mg−1Zn−1Sn−xSr (x = 0, 0.2, 0.4, 0.6, wt.%) was uniform, and the best corrosion resistance was obtained in 0.2% Sr, with a corrosion rate of 0.53 mm/y. This was mainly because the grain sizes of Mg−1Zn−1Sn−0.2Sr were refined. In addition, the Mg−1Zn−1Sn alloy had the ability to spontaneously form the network structure layer with micro/nanotopography, which was conducive to cell proliferation, adhesion, and spreading. In contrast, Song et al. [38] found that the Sr addition significantly deteriorated the corrosion performance of the as−cast Mg−Zn−Ca, as shown in Figure 3(b1,b2) with the degradation rates of 0.07 to 0.24 mm/y, respectively. This is mainly

due to the precipitation of secondary−phase particles to form more micro−couples. Thus, the addition of Sr should be controlled.

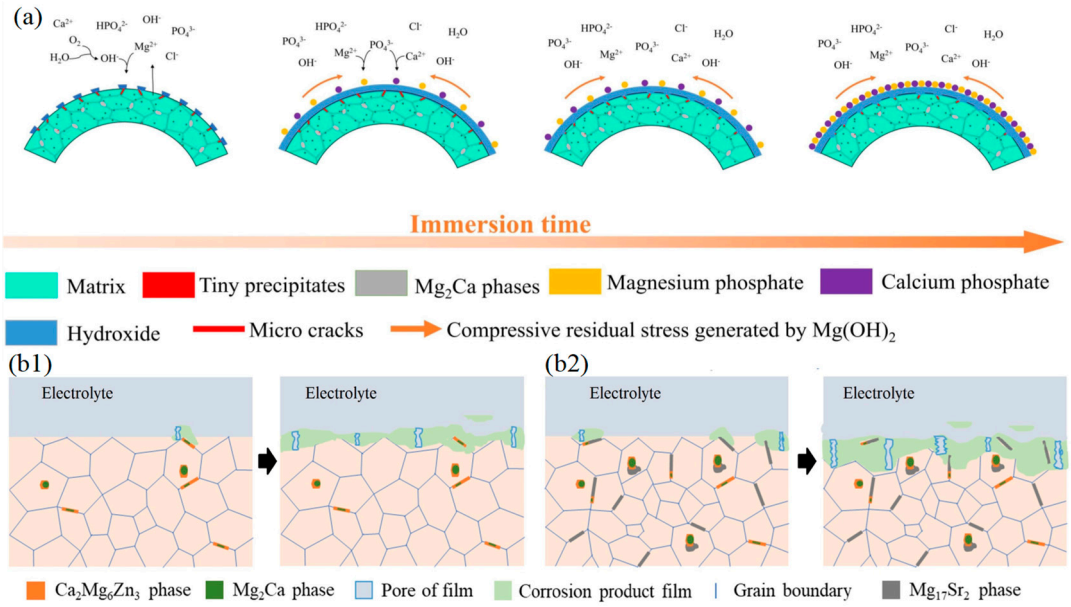

Figure 3. (**a**) Schematic diagrams illustrating the corrosion process of bent Mg−Ca−La alloys [33]; schematic illustration of Sr addition on the microstructure and corrosion process of the (**b1**) Mg−Zn−Ca and (**b2**) Mg−Zn−Ca−Sr alloys [38]. Reprinted with permission from refs. [33,38]. Copyright 2022 Elsevier.

Acting as the nutrient element for metabolism, Mn can affect the corrosion resistance of Mg alloys through the formation of the second phase/compound and the stable oxide−layer. Cho et al. [39] verified the degradation behavior of squeeze−cast Mg−Zn−Ca−*x*Mn (*x* = 0, 0.4, 0.8) for biomedical applications in vitro and in vivo. The results indicated that the corrosion resistance of squeeze−cast alloys showed improvement at higher Mn levels, due to the more refined and uniform dendritic microstructure, which was beneficial to improving the corrosion resistance. Moreover, the Mg−4Zn−0.5Ca alloy implanted into the skulls and spines of Sprague−Dawley rats for 4 weeks showed no swelling. This was because the pH of the extracted−solute decreased with the increase in Mn concentration, thus the cell viability increased. Meanwhile, Li et al. [40] assessed the effect of degradable Mg alloys supplemented with Mn on osteogenesis in vitro and in vivo. Results showed that compared with the Mg−3Zn Mg alloy, the corrosion rate of Mg−2Zn−1Mn was reduced to 0.36 mm/y. In addition, Mg−2Zn−1Mn implanted into the femur of rats showed stable degradation. It was associated with the densification degradation film and a refined microstructure with Mn addition.

3.2. Rare−Earth Elements

Compared with nutrient elements, RE elements could play an important role in improving the service properties of the Mg−based alloys, due to its unique peripheral electronic structure and rare earth energy. Furthermore, the RE elements could form intermetallic compounds and hydroxide/oxide on the surface, which weaken the negative−polarity during galvanic corrosion. More importantly, RE possess a special affinity with biomolecules to participate in metabolism reactions, which can activate or inhibit a variety of enzymes. Recently, RE elements were mainly composed of light and heavy rare−earth elements (LREs and HREs).

Light−rare−earth elements (LREs) used in medical Mg alloys primarily include Nd, Ce, and La. For example, Zhang et al. [41] systematically studied the degradation behaviors of Mg−*x*Nd (*x* = 0, 0.5, 2, 5, wt.%) in a DMEM + 10% FBS solution. Their results indicated

that with prolonged corrosion, corrosion rates first increased and then decreased, and the maximum was reached at 2%Nd. This was mainly due to the existence of intermetallic particles of $Mg_{41}Nd_5$, which caused micro−galvanic corrosion as the content gradually increased by 2%. With further addition (5%), the degradation products on the surface of Mg−*x*Nd alloys mainly included carbonates, calcium−phosphate, neodymium oxide, and neodymium hydroxide, which favored the formation of a continuous and compact corrosion layer. Afterward, Wang et al. [42] compared the corrosion of as−cast Mg−5 wt.% Nd and Mg−30 wt.% Nd in a 0.9 wt.% NaCl solution. They indicated that the corrosion current densities of the Mg−Nd alloy increased as the Nd contents increased. Due to its negative potentials, $Mg_{12}Nd$ corroded first in comparison with α−Mg, suggesting the anodic role of the phase at the initial stage. Wang et al. [43] investigated the corrosion resistance of a Mg−1.5Sn−0.5Ca alloy with and without Ce microalloying in a 3.5 wt.% NaCl solution, with corrosion rates of 4.31 and 3.12 mm/y, respectively. They indicated that Ce can refine the eutectic structure between CaMgSn and the α−Mg grains. The corrosion products were mainly $Mg(OH)_2$ and a small amount of $Ce(OH)_2$ and CeO_4, which was beneficial to enhancing the compactness of the film via the addition of Ce. Thus, the corrosion rate was reduced. Wang et al. [44] compared the degradation behaviors of the twin−roll casting of Mg−10La/20Ce with AZ31 in a 3.5% NaCl solution. The results demonstrated that the degradation rates of Mg−RE alloys were slower than that of AZ31. This was primarily because the addition of Ce/La to the Mg−based alloy was beneficial for forming amorphous alloys, which had superior corrosion resistance to crystalline alloys due to the absence of grain boundaries and precipitations.

Heavy−rare−earth elements (HREs) used in medical Mg alloys primarily include Gd, Y, and Dy. Kania et al. [45] studied the corrosion resistance of as−cast Mg−(5−*x*)Ca−1Zn−*x*Gd (*x* = 1, 2, 3 wt.%) in a Ringer's solution. The results illustrated that Mg−4Ca−1Zn−1Gd had the highest corrosion rate due to the high contents of rich−Ca phases (Mg_2Ca), which accelerated the anodic kinetics. Cheng et al. [46] reported that the corrosion resistance of the melting−casting of Mg−Zn−Ca−Y in Hanks' solution was continuously improved with the increase in Y contents. The α−Mg grains were refined gradually with the increase in Y contents and the secondary phase $Mg_{24}Y_5$ changed into fine particles with a uniform distribution. Furthermore, Y could purify the Mg−melt and reduce the intensities of galvanic corrosion caused by the second phase or impurities. Li et al. [47] analyzed the degradation behavior of Mg−2Zn−0.5Zr with different Dy contents. The results indicated that when the Dy content was less than 1.5%, the corrosion was mainly filiform corrosion. When the Dy content was above 1.5%, pitting corrosion occurred. In addition, the corrosion behavior of Mg−RE (Mg−0.3Ce, Mg−0.41Dy, Mg−0.63Gd, Mg−1.44Nd, Mg−1.43La) in 3.5%NaCl was compared by Azzeddine [48]. The corrosion resistance of Mg−RE alloys was ranked as follows: Mg−1.43La, Mg−1.44Nd, Mg−0.3Ce, Mg−0.63Gd, and Mg−0.41Dy. This was because the formation of Dy_2O_3 prevented the Mg−0.41Dy alloy from undergoing pitting corrosion.

Compared with single−rare−earth elements, double−rare−earth elements can be formed and produce a greater passivation effect, which further improves their corrosion resistance. For example, Dvorský et al. [49] found the corrosion rates of Mg−3Nd−0.5Zn, Mg−2Y−1Zn, and Mg−4Y−3Nd were 1.3, 2.4, and 0.3 mm/y. Mg−4Y−3Nd had the lowest corrosion rate due to the formation of relatively stable $Y_2O_3/Y(OH)_3$, which helped to create more protective barriers. Prasad et al. [50] also reported the role of La addition in enhancing the corrosion resistance of as−cast Mg−10Dy in a 0.9 wt.% NaCl solution. The corrosion rate of the Mg−10Dy alloy was reduced from 5.26 to 2.28 mm/y with the addition of 0.7 La. This was ascribed to the presence of Mg_{12}(Dy, La), which was less detrimental than the $Mg_{24}Dy_5$. The La/Dy addition promoted the formation of an oxide film, which enhanced the corrosion resistance of the alloys.

3.3. Other Elements

In addition to the common elements and RE elements mentioned above, the addition of Cu, Ag, Li, and Sc also affects the degradation behavior of medical Mg alloys. Cu is not only an important trace element for many enzymes in the human body but also its ions can enhance antibacterial activity. Firstly, Lotfpour et al. [51] reported that the corrosion resistance of biodegradable cast Mg−2Zn with the addition of 0.1% Cu in simulated body fluid (SBF) was enhanced. The reason was found to be related to grain refinement, the formation of a better passive layer, and the presence of a low volume fraction of MgZnCu intermetallics that created lower Volta potential differences with the α−Mg phase. In addition, Qiao et al. [52] evaluated the corrosion behavior of biodegradable Mg−2Zn−1Gd−0.5Zr−*x*Cu (*x* = 0, 0.1, 0.3, 0.5 wt.%) in Hanks' solution, with the corrosion rates of 0.09, 0.24, 0.31, and 1.10 mm/y, respectively. The reduction in the corrosion rate was due to the fact that Cu was a low hydrogen overvoltage impurity that can cause galvanic corrosion (Figure 4). Nevertheless, the Mg−2Zn−1Gd−0.5Zr−0.1Cu degradation rate was much lower than other alloys containing−Cu, making it a potentially degradable antibacterial biomaterial.

Ag is an important trace element with good biological safety in the human body, which has been successfully applied in wound healing and implant fields. For example, Liu et al. [53] explored the degradation behavior of Mg−*x*Ag (*x* = 2, 6, 8 wt.%) sheets, and the lowest degradation rate was obtained in Mg−2Ag. Subsequently, Ma et al. [54] studied the corrosion behavior of quaternary Mg−1Zn−0.2Ca−*x*Ag (*x* = 1, 2, 4 wt.%) wires applied as degradable anastomotic nails in simulated body fluid. The results showed that the corrosion resistance decreased as the Ag content increased due to the large number of fractions of $Ag_{17}Mg_{54}$, which exhibit a remarkable difference in Volta potentials compared to the α−Mg matrix.

The Li element can change the hexagonal close−packed (hcp) structure of Mg alloys into a body−centered cubic (bcc) structure, and Li^+ ions can also promote bone formation and enhance bone density in vivo. For example, Li et al. [55] analyzed the corrosion behaviors of Mg−*x*Li alloys in a 0.1 M NaCl solution with various Li contents (1, 3, 5, wt.%). The mass loss results indicated that corrosion rates determined for Mg−1Li, Mg−3Li, and Mg−5Li immersed for 3 days were 2.7, 1.9, and 1.5 $mg{\cdot}cm^{-2}{\cdot}d^{-1}$, respectively. This was due to the fact that grains with normal orientations along the {0110} and {1210} plane were difficult to corrode in Mg−5Li compared with the 45° base (0001) plane in Mg−1Li, leading to the high corrosion resistance of Mg−5Li. Meanwhile, the high Li concentration in Mg−5Li accelerated the deposition of Li_2CO_3 compounds on the surface, and the insoluble Li_2CO_3 compounds further seal the porous $Mg(OH)_2$, mitigating the permeation of aggressive Cl^- to destroy the surface film. On this basis, Xia et al. [56] investigated the corrosion behavior of biodegradable Mg−(3.5, 6.5 wt.%)Li−*x*Ca in Hanks' solution. The results pointed out that after the addition of Li and Ca, all OCP and E_{corr} values were not significantly different than the pure Mg. However, the corrosion rates were significantly higher. The main reason was that the Mg−3.5Li−*x*Ca alloy was dominated by the α−Mg phase, the Mg−6.5Li−*x*Ca alloy was dominated by the α−Mg phase and β−Li phase, and the presence of a large number of second phases resulted in an increase in the corrosion rate. In addition, the appropriate amount of Li was added and a Li_2CO_3 protective layer was formed to achieve better corrosion resistance.

Sc has the same crystal structure as Mg and has a relatively high hydrogen evolution overpotential, thus containing−Sc Mg−based alloys that showed a relatively low degradation rate. For example, Baek et al. [57] examined the corrosion resistance of HP−Mg and Mg−0.05Sc in a 0.6 M NaCl solution, and the weight−loss rates after 3 days were 4.9 and 0.36 mm/y, respectively. This was because the less noble $ScFeSi_2$ formed in Mg−Sc instead of the nobler Fe_3Si particles, thereby the degree of micro−galvanic corrosion between the anodic Mg and surrounding particulate cathodic phases was significantly diminished and the integrity of the passive layer was enhanced. Moreover, this contributed to lowering the anodic Mg dissolution rate by suppressing defect formation on the passive

layer, which resulted in relatively uniform corrosion behavior. The corrosion behaviors of Mg−2Zn−0.2Zr−*x*Sc (*x* = 0, 0.2, 0.4, 0.6, 0.8 wt.%) with the addition of Sc were also enhanced, which was investigated by He [58]. The results showed that the degradation rate of Mg−2Zn−0.2Zr−0.2Sc was 0.77 mm/y, and with an increase in the Sc element, the corrosion rate increased to 1.10 mm/y, but it was still lower than the alloy without Sc. This is due to the dispersion distribution of fine, rod−like Mg(Zn, Sc, Zr) phases leading to uniform corrosion. Furthermore, the surface potential difference between of α−Mg phase with Mg(Zn, Sc, Zr) phases was lower than with Mg(Zn, Zr) phase, improving the electrochemical homogeneity. Conversely, the addition of Sc may lead to discontinuous second precipitates, which caused the corrosion resistance to deteriorate. For instance, Yang et al. [59] studied the effect of Sc/Sm microalloying in Hanks' solution on the properties of as−cast Mg−2Zn−0.3Ca alloys. Results showed that the corrosion rates of Mg−2Zn−0.3Ca, Mg−2Zn−0.3Ca−Sc, and Mg−2Zn−0.3Ca−Sm alloys were 3.05, 4.21, and 1.26 mm/y, respectively. The precipitates distributed along the grain boundary were discontinuous, and the corrosion type of Mg−2Zn−0.3Ca−Sc was primarily intragranular corrosion, as depicted in Figure 4(b1–b3). Moreover, the corrosion was transmitted across grain boundaries to neighboring grains and spread along with the absence of a corrosion barrier, so corrosion resistance was reduced.

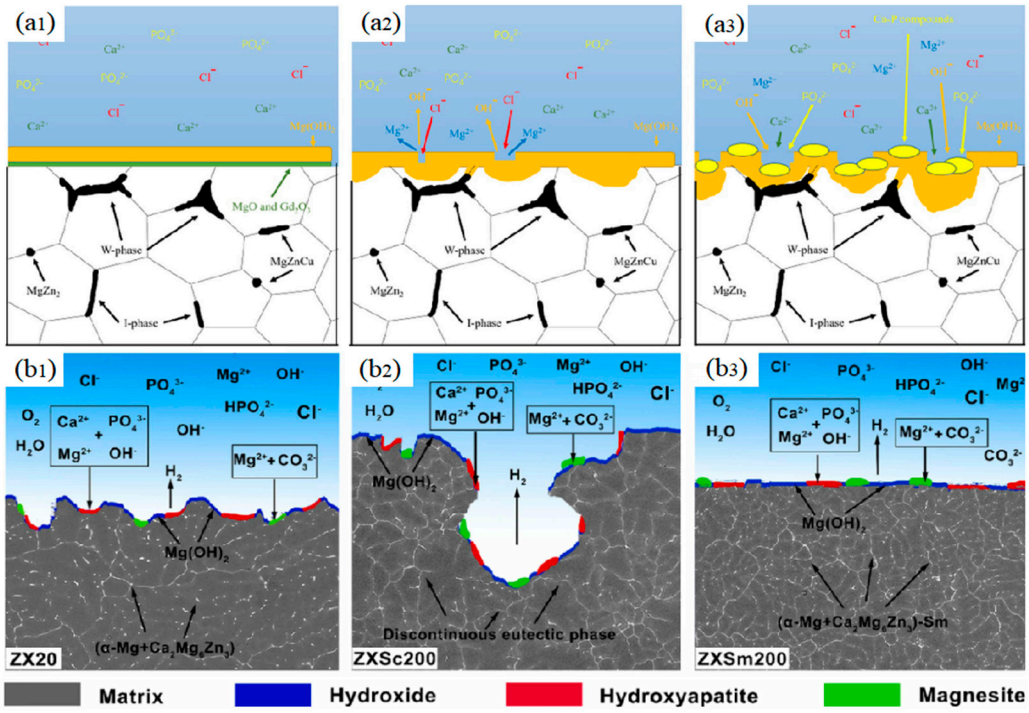

Figure 4. The corrosion mechanism of Mg−2Zn−1Gd−0.5Zr−0.1Cu alloy in Hanks' solution: (**a1**): Mg degradable and $Mg(OH)_2$ formation, (**a2**): $Mg(OH)_2$ dissolution, (**a3**) HA formation [52]; schematic illustration of corrosion mechanisms of the as−cast alloys immersion in Hanks' solution: (**b1**) Mg-2Zn-0.3Ca, (**b2**) Mg-2Zn-0.3Ca-0.4Sc, (**b3**): Mg-2Zn-0.3Ca-0.4Sm [59]. Reprinted with permission from refs. [52,59]. Copyright 2022 Elsevier.

4. Heat−Treatment

The heat−treatment process can eliminate segregation defects, reduce stress distribution, and promote recrystallization behavior. In accordance with these specific purposes, it can be roughly divided into homogenization, solution, and aging treatments.

4.1. Homogenization−Treatment

Homogenization treatment is generally carried out to reduce solute segregation and dissolve these precipitations, which has a huge effect on the biocorrosion resistance of Mg alloys. For instance, Xu et al. [60] studied the effect of homogenization on the corrosion behaviors of as−cast Mg−Zn−Y−Gd−Zr alloys in Hanks' solution, and the average corrosion rates of the as−cast and homogenized alloys were 3.49 and 2.7 mm/y. This was associated with the existence of large semi−continuous and inhomogeneous W phases ($Mg_3Zn_3Y_2$), which were liable to cause intense galvanic−corrosion between the a−Mg matrix and W phases. The volume fraction of the coarse second phases in the homogenized alloy decreased, which affected the sizes and intensities of galvanic−cells, thus the corrosion resistance was improved. Similarly, Zhang et al. [61] reported that the corrosion resistance of Mg−Y in a 3.5 wt.% NaCl solution was enhanced after homogenization treatment, and the degradation morphology become more uniform as the homogenization temperature and time increased. Lv et al. [62] further revealed the effect of homogenization treatment on the corrosion resistance of a cast Mg−4Zn−1Ca alloy in Hanks' solution. The results clearly showed that the average mass loss rate determined for the as−cast and as−homogenized samples immersed in Hanks' solution for 3 days were 0.18 and 0.08 $mg{\cdot}cm^{-2}{\cdot}d^{-1}$, respectively. The corrosion initiation of the as−cast alloy occurred in the porous $Ca_2Mg_6Zn_3$ phases and gradually propagated toward the surrounding α−Mg, resulting in severe corrosion damage. However, the porous $Ca_2Mg_6Zn_3$ phases were transformed into a compact one after homogenization treatment. Although localized corrosion also occurs in as−homogenized treatment, the corrosion resistance was enhanced due to the barrier effect on the corrosion process. Moreover, as−homogenized Mg−4Zn−1Ca was more favorable for bone−related gene expression in rBMSCs.

4.2. Solution−Treatment

Solid−solution treatment can lead to the strong dissolution and lattice distortion of the as−cast alloys, which affects the microstructure evolution and corrosion behavior significantly. For example, Janbozorgi et al. [63] evaluated the corrosion resistance of medical Mg−2Zn−1Gd−1Ca via solution treatment in simulated body fluids. The results revealed that the corrosion rate was reduced from 3.09 to 1.35 mm/y. The main reason for the low corrosion resistance in the as−cast alloy was the strong galvanic corrosion of α−Mg together with the dendritic microstructure and micro−area segregation. The formation of intense lattice distortion and the strong dissolution of precipitates after the solution treatment can induce the enhancement of corrosion resistance. Gui et al. [64] further proved that solid solution treatment can improve the corrosion behavior of Mg−5Y−2Nd−3Sm−0.5Zr in a 3.5% NaCl solution at the rate of 1.3 to 0.4 $mg{\cdot}cm^{-2}{\cdot}h^{-1}$. This was mainly due to the complete dissolution of the skeletal structure, the uniform surface, and the lack of impurity aggregation on the grain boundaries. As a result, the corrosion resistance of the alloy after solution treatment was enhanced. The corrosion resistance of Mg−2Cu and Mg−5Cu alloys after solid solution treatment in Hanks' balanced salt solution was also verified by Yan [65]. The enhanced corrosion resistance was owing to the remarkable decrease in Mg_2Cu contents after solution treatment. The distribution of the Mg_2Cu phase changed from dispersion to localization, which lead to a large cathodic phase coupled with a small matrix anode in the local region. Furthermore, Iranshahi et al. [66] investigated the degradation rate of a solution heat−treated ZKX50 alloy in a 0.5 wt.% NaCl solution, with corrosion rates of 0.46 and 0.73, respectively. They primarily observed the partial dissolution and spheroidizing of $Ca_2Mg_6Zn_3$ IMPs particles, and the morphology of intermetallic changed from strip−like to globular, which decreased the contact area between $Ca_2Mg_6Zn_3$ as the cathode and the matrix as the anode.

Furthermore, Cao et al. [67] analyzed the effect of solution treatment on the corrosion behavior of as−rolled Mg−5Gd in a 3.5 wt.% NaCl solution. The results stated that the corrosion rate decreased from 4.60 to 1.48 mm/y. This was because, after solution treatment, the deep corrosion cavities were absent as the large cathodic particles dissolved

into the matrix, which only left a few fine particles. Thus, the strong micro−galvanic corrosion was significantly minimized. Moreover, Jiang et al. [68] studied the corrosion resistance of extruded Mg−2Zn−1Mn treated by solid−solution treatment in Ringer's solution. The results showed that the degradation rate of the solution−treated alloy was reduced from 0.48 to 0.44 mm/y, and the T4−treated sample (solution treatment) showed less corrosion product than the extruded sample. It can be speculated that the volume fraction of Mg_xMn_y decreased significantly after T4, and the fraction of dislocations and defects decreased. Thus, the T4−treated alloy showed higher corrosion resistance than the extruded alloy. Dong et al. [69] studied the effect of solution treatment on the corrosion behavior of the as−extruded Mg−Sr alloy in Hanks' solution. The results found that after the solution was exposed to T4−450 °C, the corrosion rate of the extruded alloy was changed from 0.149 to 0.107 mm/y, but at T4−560 °C, the corrosion rate increased slightly to 0.153 mm/y. Moreover, Kang et al. [70] studied the corrosion resistance of the medical as−extruded Mg−Zn−Y−Nd alloy via solution−treatment. The results found that the corrosion resistance of the treated alloy solution was obviously superior to as−extruded alloys, and the minimum corrosion rate was 0.5 $mg \cdot cm^{-2} \cdot d^{-1}$. This was primarily because the grain size of the alloy was further homogenized after heat treatment, and some grain boundaries dissolved into the matrix, which reduced the galvanic−cells and impeded the local corrosion. Furthermore, the heat treatment process may remove the residual stress, which further inhibited the corrosion rates.

In addition, it can improve the corrosion resistance after the solution treatment, and the partial dissolution of the second phase will also increase the corrosion rate. For example, Chelliah et al. [71] found that the corrosion rate of as−cast AZ91 was reduced by 72% compared to the T4−treated alloy in Ringer's solution. This was because the passive film of as−cast AZ91 contains $MgCO_3$ and $CaCO_3$ precipitates, while the treated−T4 AZ91 was primarily composed of unstable $Mg(OH)_2$. The corrosion products were more compact and protective than the latter. Furthermore, the larger area fraction of the β−$Mg_{17}Al_{12}$ phase in as−cast alloys could act as an effective barrier to biocorrosion. Similarly, Del Rosario Silva Campos et al. [72] also reported the effect of solution treatment on the corrosion behavior of as−cast Mg−10Gd in a 0.5% NaCl solution. The results indicated that the corrosion rate of the solution−treated alloy was twice that of the as−cast one, with corrosion rates of 5.0 and 10.0 mm/y, respectively. The relatively good corrosion behavior in the as−cast condition was associated with the formation of Gd enrichment zones, which reduced the local damage due to galvanic corrosion between the Mg_5Gd phase and the α−Mg matrix. However, the T4 heat treatment caused the Gd to distribute uniformly in the matrix, and the Mg_5Gd phase was dissolved, while the existence of the GdH_2 phase also reduced the corrosion resistance.

4.3. Aging−Treatment

Compared with the solid−solution treatment, the aging treatment can improve the corrosion resistance of the alloy by forming nano−scale precipitations. Janbozorgi et al. [63] also studied the corrosion resistance of aging treatment of medical Mg−2Zn−1Gd−1Ca in simulated body fluid. The results showed that the corrosion rate of the alloy was reduced from 3.09 to 1.85 mm/y. This was mainly due to the appropriate precipitation of the $Ca_2Mg_6Zn_3$ and $Mg_3Gd_2Zn_3$ secondary phases during aging treatment, which induced the enhancement of corrosion resistance in the heat−treated samples. Gui et al. [64] studied the effect of aging treatment on corrosion behaviors of as−cast Mg−5Y−2Nd−3Sm−0.5Zr in a 3.5% NaCl solution. The results showed that as the aging time increased, the corrosion rate decreased from 1.3 as cast to 0.3, 0.2, and 0.5 $mg \cdot cm^{-2} \cdot h^{-1}$. Therein, when the aging time was 12 h, the lowest weight loss rate of the Mg−5Y−2Nd−3Sm−0.5Zr alloy in 3.5% NaCl was achieved. Unlike solid−solution treatment, the corrosion resistance of aging treatment improved due to the fine precipitation phase and the dispersion distribution in the matrix, which can inhibit the formation and expansion of corrosion. Li et al. [73] studied the degradation behavior of the Mg−5.8Zn−2.0Yb−0.5Zr alloy during aging treatment in

the simulated body fluids. The results indicated that after peak−aged (PA), under−aged (UA), and over−aged (OA) durations, the corrosion rates were 2.3, 23.5, and 58.6 mm/y, respectively. This was because the denser and more homogeneous nanoprecipitates result in a more compact and more stable protective film, thereby possessing better corrosion resistance. Subsequently, similar experimental results for Mg−1Zn−1Ca in Hanks' solution were further verified by Pulido−González [74].

Compared with single aging treatment, aging treatment after solution treatment can further reduce the degradation rate. For example, Cao et al. [67] compared the influence of solution treatment on the corrosion behavior of rolled Mg_5Gd alloys in a 3.5 wt.% NaCl solution. The results showed that the aging process after solution treatment further decreased the corrosion rate to 1.40 mm/y. This was because the aging process after solution treatment precipitated nano−sized Mg_5Gd particles, which formed a protective product layer. However, some aging treatments will produce a large amount of precipitation, which will increase the corrosion rate. For example, Jiang et al. [68] studied the effect of aging treatment (T5) on the corrosion resistance of an extruded Mg−2Zn−1Mn alloy in Ringer's solution. The results showed that the degradation rate of the T5−treated alloy increased to 0.50 mm/y, and the surface presented a typical filament corrosion morphology. This is because, in the process of T5 treatment, Zn and Mg precipitate at the grain boundary of the extruded alloy, forming Mg_7Zn_3 phases. Mg_7Zn_3 phases can act as micro−cathodes and the alloy surface showed an apparent micro−galvanic effect to accelerate the corrosion rate. Nevertheless, as for these alloys, each sample was degraded below 0.5 mm/y. In addition, Dong et al. [69] studied the effect of aging treatment on the corrosion behavior of an as−extruded Mg−Sr alloy in Hanks' solution. Results showed that after aging, the corrosion rate of the extruded alloy changed from 0.149 to 0.174 mm/y, and with the increase in aging time, the corrosion rate further increased to 0.318 mm/y. This is primarily because, after aging treatment, the $Mg_{17}Sr_2$ precipitation with large quantities increased galvanic corrosion and accelerated the corrosion rates. In addition, the changes in corrosion resistance of Mg alloys after different heat treatments are presented in Table 1.

Table 1. Changes in corrosion resistance of common magnesium alloys after different heat treatments (HT: Homogenization−treatment; ST: Solution−treatment, A: Aged−treatment).

Alloy	Condition	Second Phase(s)	Testing Environment	Corrosion Resistance	Reference
Mg−2.5Zn−0.7Y−0.7Gd−0.4Zr	HT	$Mg_3Zn_3Y_2$	Hanks' solution	↑	[60]
Mg−Y	HT	$Mg_{24}Y_5$	3.5 wt.% NaCl solution	↑	[61]
Mg−4Zn−1Ca	HT	$Ca_2Mg_6Zn_3$	Hanks' solution	↑	[62]
Mg−2Zn−1Gd−1Ca	ST	$Ca_2Mg_6Zn_3$, $Mg_3Gd_2Zn_3$	SBF solution	↑	[63]
Mg−2Zn−1Gd−1Ca	A	$Ca_2Mg_6Zn_3$, $Mg_3Gd_2Zn_3$	SBF solution	↑	[63]
Mg−5Y−2Nd−3Sm−0.5Zr	ST	$Mg_{24}Y_5$ $Mg_{41}Nd_5$ $Mg_{41}Sm_5$	3.5% NaCl solution	↑	[64]
Mg−5Y−2Nd−3Sm−0.5Zr	A	$Mg_{24}Y_5$ $Mg_{41}Nd_5$ $Mg_{41}Sm_5$	3.5% NaCl solution	↑	[64]
Mg−2Cu/ Mg−5Cu	ST	Mg_2Cu	Hanks' balanced salt solution	↑	[65]
ZKX50	ST	$Ca_2Mg_6Zn_3$	0.5 wt.% NaCl solution	↑	[66]
Mg−3.0Gd−2.7Zn−0.4Zr−0.1Mn	ST	$(Mg, Zn)_3Gd$	Hanks' solution	↑	[67]
$Mg_{91.5}Al_{3.5}Gd_5$	ST	Mg_5Gd, $Mg_{12}ZnY$, Al_2Gd	1 wt.% NaCl	↑	[67]
$Mg_{91.5}Al_{3.5}Gd_5$	ST + A	Mg_5Gd, $Mg_{12}ZnY$, Al_2Gd	1 wt.% NaCl	↑	[67]

Table 1. *Cont.*

Alloy	Condition	Second Phase(s)	Testing Environment	Corrosion Resistance	Reference
Mg_5Gd	A	—	3.5 wt.% NaCl saturated with $Mg(OH)_2$	↓	[67]
Mg_5Gd	ST	—	3.5 wt.% NaCl saturated with $Mg(OH)_2$	↑	[67]
Mg_5Gd	ST + A	—	3.5 wt.% NaCl saturated with $Mg(OH)_2$	↑	[67]
Mg−2Zn−1Mn	HT	Mg_xMn_y	Ringer's solution	↑	[68]
Mg−Sr	HT	$Mg_{17}Sr_2$	Hanks' solution	↑, then↓	[69]
Mg−Y−Zn−Mn	ST	LPSO	3.5 wt.% NaCl	↑	[70]
AZ91	ST	$Mg_{17}Al_{12}$	Ringer's solution	↑	[71]
Mg−10Gd	ST	GdH_2 Mg_5Gd	0.5% NaCl solution	↑	[72]
Mg−Zn−Ca	ST	Mg_2Ca, $Ca_2Mg_6Zn_3$	Hanks' solution	↑	[74]
Mg−Zn−Ca	Peak−A	Mg_2Ca, $Ca_2Mg_6Zn_3$	Hanks' solution	↓	[74]
Mg−Zn−Ca	Over−A	Mg_2Ca, $Ca_2Mg_6Zn_3$	Hanks' solution	↑	[74]

5. Plastic−Deformation

Compared with heat treatment and micro−alloying, plastic processing can further improve the corrosion resistance of medical Mg alloys via grain refinement, crushing the precipitations, and decreasing the microstructure defects.

5.1. Rolling−Deformation

The rolling process is the most important method of forming metal materials at present, so it is necessary to study the corrosion behaviors of Mg alloys via rolling, particularly in high−strain−rate, high−reduction, and high−temperature conditions. For example, Guo et al. [75] studied the effects of the rolling strain rates on the biocorrosion behavior of Mg−5Zn−1Mn in Hanks' solution. The results showed that the average rolled strain rate was fixed at 10, 15, and 20 s^{-1} and the corrosion rates were 0.72, 0.63, and 0.54 mm/y, respectively. As the strain rate increased, the corrosion morphology transitioned from severe pitting to uniform filiform−corrosion. It can be speculated that as the dynamic recrystallization (DRX) volume fractions increased, the area−ratio of the cathode and anode was reduced, resulting in less severe galvanic corrosion. Furthermore, the dislocation density was decreased with increasing DRX volume fractions, which was also beneficial to the corrosion resistance. Similarly, the improvement in corrosion resistance for Mg−2Zn−2Er−0.3Zr−0.3Mn was explored by Zheng [76], in which they were treated by various rolling reductions (25%, 50%, and 75%). The results revealed that severe localized corrosion was found on HR−25, while HR−50 and HR−75 revealed uniform corrosion and filiform corrosion. The worst corrosion resistance of HR−25 was due to the generation of twins, and the deformation of−twins increased the galvanic corrosion. The superior corrosion resistance of HR−50/HR−75 was associated with the homogeneous structure and fine−grain, which can reduce the hydrogen chemical kinetics, protect the film−layer integrity, and insulate the contact reaction between corrosive ions and the α−Mg matrix. In addition, Deng et al. [77] found that the corrosion properties of WE43 improved when treated with different rolling−temperatures. This was primarily because, when the temperature was low, the second phase was coarser, resulting in a large number of dislocation defects, and the formation of a large number of galvanic double layers. As the rolling

temperature increased, the segregation degree decreased and the grains were markedly refined, resulting in uniform corrosion morphology.

Compared with the ordinary rolling process, the large plastic deformation of the twin roll casting (TRC) process can achieve a finer−grained microstructure. At the same time, it can form a unique structure to further protect the surface oxide film and improve its corrosion resistance. For example, Wang et al. [78] investigated the corrosion behavior of the twin roll casting Mg−RE in the PBS solution. The results declared that after twin roll casting, the corrosion current densities decreased from 1.74×10^{-3} to 1.51×10^{-4} μA. After the TRC process, the cathode reaction formed a heterogeneous, thin, porous layer, which was predominantly magnesium hydrate on the surface of the Mg−RE, preventing contact between the solution and the substrate. Furthermore, the Mg−RE sheet obtained by the TRC process had a unique structure, due to its crystal structure surrounding the amorphous structure, which improved the corrosion resistance of the magnesium−hydrated film, thus the corrosion resistance was enhanced. In addition, as an implant material, the Mg−RE sheets were safe with respect to rats' physical fitness and induced new bone formation in vivo. On this basis, Dargusch et al. [79] assessed the in vivo corrosion of a rare−earth−free Mg−Zn−Ca alloy manufactured using twin roll casting (TRC) and compared it to the properties of the rare−earth (RE)−element−containing WE43 alloy. The results displayed that the TRC Mg−0.5Zn−0.5Ca alloy showed a degradation rate of 0.51 mm/y similar to that of the WE43 (0.47 mm/y) in the rat model 7d after implantation. More importantly, the rate of degradation was perceptibly lower after 4 weeks (0.27 for the TRC Mg−Zn−Ca alloy and 0.29 mm/y for WE43). The reasons are as follows: (i) After the TRC process, the refinement microstructure was obtained and the segregation degree was reduced; (ii) the slower degradation after 4 weeks of'−immersion was due to the formation of more protective film−layers (hydroxides, calcium phosphates, and MgO). Compared with WE43, the presence of more organized scarring tissue around TRC Mg−0.5Zn−0.5Ca suggests that the biodegradation of the RE−free alloy may be more conducive to the tissue proliferation and remodeling process.

5.2. Extrusion−Deformation

Extrusion is another common process for metals, especially for magnesium and zinc alloys. The fine structure and the broken second phase that formed after extrusion could promote the formation of a dense oxide film−layer on the surface, thus reducing micro−galvanic corrosion. For example, Xu et al. [60] found that the corrosion resistance of the Mg−Zn−Y−Gd−Zr alloy in Hanks' solution was enhanced after the extrusion process, and the corrosion rates decreased from 1.05 to 0.616 mm/y. This was because, after hot extrusion, the W phase changed, thus the area ratio between the anode and the cathode and the intensity of micro−galvanic corrosion in the as−extruded alloy was the lowest. Furthermore, the refined microstructure increased the volume fraction of grain boundaries. The chemical activity of the grain boundary is higher than that of the matrix, which can rapidly offer many more nucleation−sites for production deposition, thus improving the corrosion resistance of the studied alloys. Compared with other influence factors, the optimum corrosion resistance of Mg alloys could be achieved by increasing the extrusion temperature. Cao et al. [80] analyzed the corrosion behavior of Mg−2Y−1Zn−0.4Zr−0.3Sr with various extrusion temperatures in simulated body fluid conditions. The results revealed that the as the temperature increased from 300 to 450 °C, the corrosion rates were 1.3, 0.78, 0.47, and 0.55 mm/y, respectively. The increase in the extrusion temperature reduced the precipitation intensity of the W−phase and decreased the galvanic−cells, which weakened the occurrence of galvanic−corrosion sites, improving the corrosion resistance. In addition, the potential of grain boundaries is higher than that of adjacent grains, which also plays a role in preventing corrosion diffusion. Therefore, as the extrusion temperature increased to 400 °C, the galvanic sites and intensities were weakened. Xu et al. [81] further investigated the effect of the extrusion temperature on the corrosion behavior of Mg−2Zn−1Gd−0.4Mn−0.1Sr in Hanks' solution. The results showed that

for extrusion at 320 °C, 360 °C, and 400 °C, the corrosion rates of the alloys were 0.117, 0.094, and 0.107 mm/y, respectively, and the lowest corrosion rate and uniform degradation model was achieved at an extrusion temperature of 360 °C. It can be speculated that as the extrusion temperature increases, the bimodal grain structure transforms into a uniform microstructure with the equiaxed grains, and the volume fractions of W precipitates decrease (as shown in Figure 5). In addition to the conventional extrusion process, Shunmugasamy et al. [82] studied the corrosion response on friction stir extrusion (FSE) of an ultra−thin wall biodegradable Mg alloy in Hanks' balanced salt solution. The results indicated that after the FSE process, the corrosion rates of the alloy decreased from 16.4 to 8.3 mm/y. This was because the grains were obviously refined after extrusion, and the corrosion rate was reduced. Meanwhile, the inner tube surface with refined grains and a basal texture resulted in micro−galvanic corrosion, and coupled with the outer tube surface, it resulted in localized dissolution preferentially initiating on the outer surface. Equal−channel angular pressing (ECAP) is one of the most efficient techniques to fabricate fine−grained metallic materials, and the corrosion rate can be reduced by further refining the grains and increasing the grain boundary density. For example, Ly et al. [83] studied the effect of equal−channel angular pressing as pretreatment on the corrosion behavior of biodegradable Mg−Zn−Ca in Hanks' solution. The results showed that the corrosion rates of the as−cast and ECAP alloys after 36 days of immersion were 0.830 and 0.597 mm/a, respectively. This was primarily because the ECAP treatment resulted in grain refinement and the enhanced formation of the corrosion product layer on the Mg alloy surface as a result of the increased grain boundary density. Subsequently, Horky et al. [84] investigated the effects of double equal−channel angular pressing (D−ECAP) on the microstructure and degradation behavior in simulated body fluid. The results showed that after D−ECAP, Mg−Zn−Ca exhibited low degradation rates and smooth surfaces. This was due to grain refinement during D−ECAP, which occurs via dynamic recrystallization, and only the presence of Mg_2Ca intermetallic particles. Therefore, the D−ECAP−treated alloy exhibits good degradation properties, which makes it a promising candidate for the future as an absorbable orthopedic implant material. On this basis, Kavyani et al. [85] studied the corrosion behaviors of Mg−Zn−Ca−Mn under different extrusion conditions, with one and two passes of the equal−channel angular pressing (HECAP) process in simulated body fluid. The results clearly revealed that after different extrusion treatments, the corrosion rate of the alloy decreased from 0.142 to 0.087, 0.074, and 0.058 mm/y, respectively, and the two−pass HECAPed sample had the highest corrosion resistance. This is because, after extrusion and HECAP, the grain size of the alloy was markedly refined due to the occurrence of dynamic recrystallization and the formation of a hydroxyapatite protective layer, which significantly improved the corrosion resistance. Meanwhile, the grain size distribution of the two−pass HECAPed sample was uniform, resulting in better corrosion resistance.

5.3. Other Plastic−Deformations

Compared with the above common processes, other plastic deformation modes such as forging, stamping, and high−pressure torsion will also affect corrosion resistance. For example, Liu et al. [86] compared the corrosion behaviors of extruded and forged WE43 in a 0.6 M NaCl solution. The results showed that after being extruded and forged, the corrosion rates were 0.7 and 1.35 mm/y, respectively. The extruded WE43 showed a uniform corrosion morphology, while the forged WE43 suffered from severe local galvanic corrosion. After extrusion deformation, the WE43 undergoes complete dynamic recrystallization with a relatively uniform distribution of second phases. However, the forged WE43 exhibited coarse grains and a larger phase size relative to the extruded WE43, along with the nonuniform segregation of rare earth elements. Furthermore, strong micro−coupling was formed between the large second phase and the Mg matrix, which caused severe local corrosion. Thus, the corrosion rate was approximately two times faster than that of the extruded−WE43.

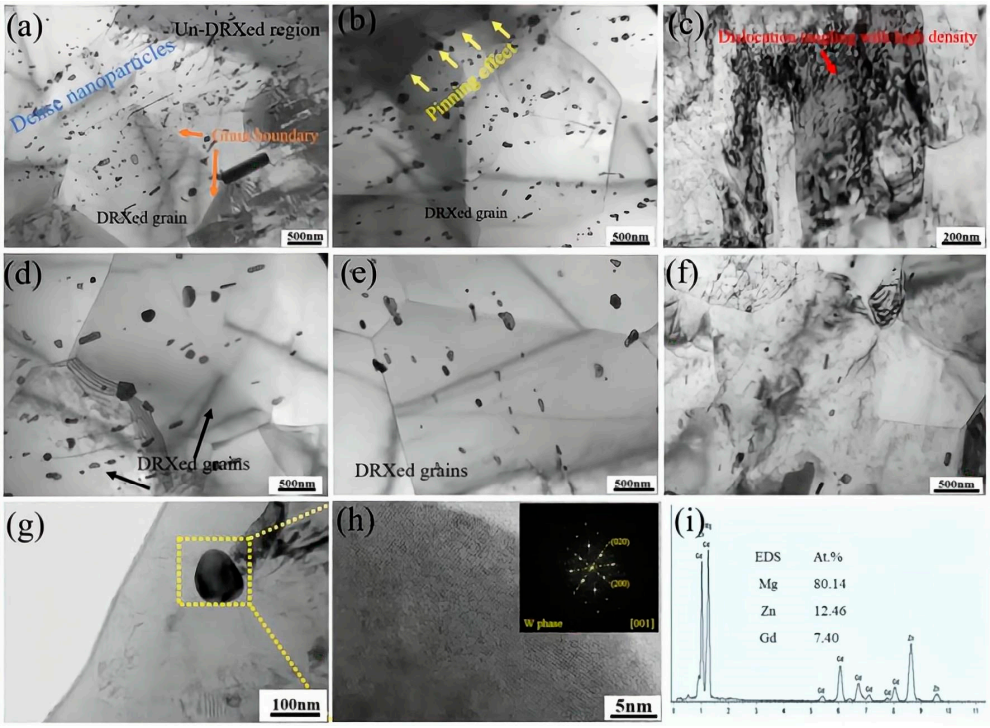

Figure 5. Schematic images of TEM bright–field (BF): (**a**,**b**) DRXed and un–DRXed regions in E320, (**c**) E320, (**d**,**e**) E360, (**f**) E400, (**g**) spherical nanoscale phase, (**h**,**i**) HRTEM micrograph, FFT image and EDS result corresponding to the nanoscale precipitate in (**g**) [81]. Reprinted with permission from ref. [81]. Copyright 2022 Elsevier.

6. Surface Modification

In addition to adjusting the corrosion resistance of the alloy by changing its own structure, surface modification is also an important means to improve the corrosion resistance of medical Mg alloys. It can improve corrosion resistance by forming a physical barrier to isolate the corrosive medium, and can also improve biological activity, antibacterial, self−healing, and other functions. At present, the most commonly used coating methods are mainly composed of mechanical surface treatment, organic/polymer coatings, inorganic coatings, and composite coatings.

6.1. Mechanical Surface Treatment

Mechanical surface treatment is mainly achieved via high−energy shot peening (HESP), without introducing other substances, and it is ultimately achieved via in−situ surface nanocrystallization (ISNC), forming nanocrystals and dense barriers to improve the corrosion resistance of medical magnesium alloys. For example, Wu et al. [87] studied the corrosion properties of a Mg−alloy bone−plate treated by high−energy shot peening (HESP) in a 0.9 wt.% NaCl solution. The results showed that after 15 min of high−energy shot peening, the corrosion rate was 0.017 $mg \cdot cm^{-2} \cdot h^{-1}$, while the corrosion rate was 0.024 $mg \cdot cm^{-2} \cdot h^{-1}$ for the untreated sample. This is due to the occurrence of mechanical twins caused by HESP. The mechanical twins can inhibit the dislocation movement, resulting in a large increase in subgrain−boundaries. Afterward, dynamic recrystallization was caused due to the distortion of energy, and finally, nano−particles were formed. At the same time, HESP generated residual compressive stress, which increased the density of the passivation film $Mg(OH)_2$, thus improving the corrosion resistance. In addition, the slightly dissolved $Mg_2Cl(OH)_3 \cdot 4H_2O$ protects the passivation film and slows the corrosion rate by reducing the free movement of surface ions and blocking the entry of media such as oxygen. Meanwhile, Guo et al. [88] studied the effect of laser shock peening on the corrosion behavior of biocompatible ZK60 in a simulated body fluid. The results showed that

with the increase in laser shot peening density, the corrosion current densities decreased from 1.378×10^{-5} to 1.267×10^{-5}, 1.230×10^{-5}, and 1.196×10^{-5} A/cm^2, respectively. This was mainly due to the increase in residual compressive stress and grain refinement. Firstly, the smaller the grain sizes, the more grain boundaries there are, which can act as a physical shield to prevent corrosion. Meanwhile, the increase in residual compressive stress on the surface of the sample made the passivation film more compact. Liu et al. [89] studied the electrochemical corrosion properties of AZ31 with laser shock peening (LSP) pretreatment in 3.5 wt.% NaCl, and the current densities of the bare and LSP alloys were 392.5 and 13.04 μA/cm^2, respectively. This was primarily due to the existence of massive grain boundaries and compressive residual stress, which acted as physical−barriers to the corrosion medium. The LSP process induced severe plastic deformation and significantly decreased the contents of the β−$Mg_{17}Al_{12}$ phase, which effectively enhanced the corrosion resistance. Additionally, the LSP pretreatment produced crystal defects and refined grains in the surface layer, which enhanced the surface activity of AZ31 and increased nucleation spots of phosphate crystals. Thus, compared to the untreated sample, the LSP−treated sample had relatively better corrosion resistance. Subsequently, Singh et al. [90] investigated the effect of soda−lime shot blasting on the corrosion resistance of AZ31 in simulated body fluids. The results indicated that the corrosion rate after the 21st day of the shot−blasting−treated sample was found to be significantly less. This is primarily due to the $Mg(OH)_2$ layer that formed on the surface of the sample, retarding the rapid corrosion of magnesium alloys.

Additionally, other surface mechanical treatments such as ultrasonic treatment and friction treatment can also affect the degradation behavior of medical Mg by improving the surface microstructure. For example, Hou et al. [91] studied the corrosion behavior of AZ31B after ultrasonic nanocrystal surface modification (UNSM) in simulated body fluid. The results indicated that the corrosion current densities slightly increased from 2.67 to 5.27 μA/cm^2 after UNSM. This was related to the increased surface area after patterning and higher dislocation density induced by UNSM, which slightly accelerated the galvanic corrosion rate. In contrast, Marchenko et al. [92] found that the corrosion resistance of Mg−4Ca−1Zn improved after ultrasonic treatment and doping with nanodiamonds. This was due to the correlation between the phase volume fractions segregated along the grain boundaries. After ultrasonic treatment, the densities of the second phase were lowest, and the degradation rate was the lowest. In addition, nanodiamond particles did not markedly affect the degradation rate, which was helpful to achieve a high biocompatibility level of the Mg alloy in contact with living organisms. Meanwhile, Long et al. [93] reported that the corrosion resistance of as−cast Mg−5Zn after friction stir processing (FSP) was enhanced in a 3.5 wt.% NaCl solution, and the corrosion current densities were reduced from 3.1×10^{-5} to 4.1×10^{-6} A/cm^2. This could be explained by the fact that after the FSP treatment, the precipitated phases in the Mg−5Zn alloy were uniformly refined and dissolved, and the corrosion product layer of the FSPed alloy was more uniform and less permeable than that of as−cast alloys. Similarly, Rokkala et al. [94] indicated that the dissolution rate of the Mg−Zn−Dy alloy after friction stir processing (FSP) improved in DMEM with a 10% FBS solution, and the degradation rate was reduced from 0.24 to 0.07 mm/y. It is mainly because the fine−grain microstructure and uniform structure of FSPed alloy improve the corrosion resistance.

6.2. Inorganic Coating

Inorganic coatings mainly include ceramic coatings and metal coatings, which can improve their degradation performance by forming dense and uniform barriers.

Commonly, ceramic coatings change the corrosion resistance of Mg alloys primarily by reducing porosity. For example, Baghdadabad et al. [95] studied the corrosion behavior of bioactive ceramic coatings synthesized by plasma electrolyte oxidation on AZ31 with different $Na_2SiO_3 \cdot 9H_2O$ concentrations in simulated body fluid. The results indicated that the excellent corrosion resistance of PEO was achieved via the concentration addition of

10%. On one hand, the increase in the corrosion resistance of the internal dense layer was due to the presence of F^-. On the other hand, $MgSiO_3$ was formed via three different reactions during the PEO process (Equations (1)–(4)). According to the following formula (Equations (1)–(4)), due to the high plasma temperature and time, reactions (1) and (2) were the formation of the dual−phase compound of Mg_2SiO_4 and SiO_2, which had transformed into $MgSiO_3$. Meanwhile, Reaction (3) was ${SiO_3}^{2-}$ and Mg^{2+} reacting to form $MgSiO_3$. Reaction (4) was the reaction of MgO and SiO_2 during the PEO process under high plasma temperatures. Thus, the sealing of the porous external layer was due to the presence of ${SiO_3}^{2-}$ and ${PO_4}^{3-}$ on the external porous layer, and the external porous layer started to seal and became compact. Thus, the corrosion resistance of the alloy was improved at the optimum concentration. On this basis, Keyvani et al. [96] assessed the corrosion behavior in Hanks' solution of ceramic coating developed on AZ31 by plasma electrolytic oxidation and ZnO nanoparticles. The results indicated that the corrosion resistance of the coating was substantially increased by increasing the concentration of ZnO nanoparticles from 0 to 6 g/L, and the I_{corr} reduced from 1.3 to 0.08 A/cm^2. This was due to the formation of the dense and compact coating achieved by the addition of 6 g/L ZnO nanoparticles. Similarly, the excellent corrosion resistance of PEO coatings was further achieved at voltages of 500 V, with a corrosion current of 7.62×10^{-8} A/cm^2 [97]. This is because as the coating deposition voltage increased, the pore density of the coating decreased and thus became more compact. Moreover, the coatings synthesized at higher voltages exhibited higher adhesive and cohesive properties owing to the greater overall thickness of the coatings, thus the corrosion resistance improved.

$$2Mg^{2+} + {SiO_3}^{2-} + 2OH^- \rightarrow MgSiO_4 + H_2O \quad (1)$$

$$MgSiO_4 + SiO_2 \rightarrow MgSiO_3 \quad (2)$$

$$Mg^{2+} + {SiO_3}^{2-} \rightarrow MgSiO_3 \quad (3)$$

$$Mg + SiO_2 \rightarrow MgSiO_3 \quad (4)$$

The metal coating improves the external defects of the coating by introducing other particles, thus improving its corrosion resistance. For example, Song et al. [98] evaluated the corrosion resistance of Mg−2Zn−Mn−Ca−Ce via equal−channel angular pressing and a hydrothermal surface coating in Hanks' solution (as listed in Figure 6). The results declared that the corrosion rate of the as−cast alloy changed from 0.625 to 0.896 mm/y after equal−channel angular pressing but decreased to 0.066 mm/y after hydrothermal coating. This is mainly due to the high density of grain boundaries, which can provide a high driving force in the hydrothermal reaction process. Li et al. [99] researched a silicate−loaded MgAl LDH coating on biomedical Mg alloys for corrosion retardation. Electrochemical tests revealed that the LDH−SiO_3 coating reduced the corrosion current density by 266 times to 0.8 μA/cm^2 in the simulated body fluid, and the average corrosion rate diminished from 4.79 mm/y of the bare alloy to 0.02 mm/y of the LDH−SiO_3 coating alloy. This was because the direct effect of the silicate precipitate was to block local defects in the coating, thus resulting in higher resistance against aggressive species. Additionally, Cl^- was trapped by the LDH coating as a result of the exchange with ${SiO_3}^{2-}$, thereby increasing the time required by Cl^- to reach the substrate, and the adherent inner LDH coating also contributed to long−term protection. Moreover, Mashtalyar et al. [100] assessed the corrosion of Ca/P−coatings in Ringer's solution. Antibacterial coatings formed on the Mg alloy via plasma electrolytic oxidation with subsequent antibiotic impregnation. The results showed that the corrosion current density of the formed coating substantially decreased compared to the bare alloy. Furthermore, the obtained coatings reduced the corrosion rate of the Mg alloy in an environment similar to human body fluid, thereby regulating the bioresorption of the implant.

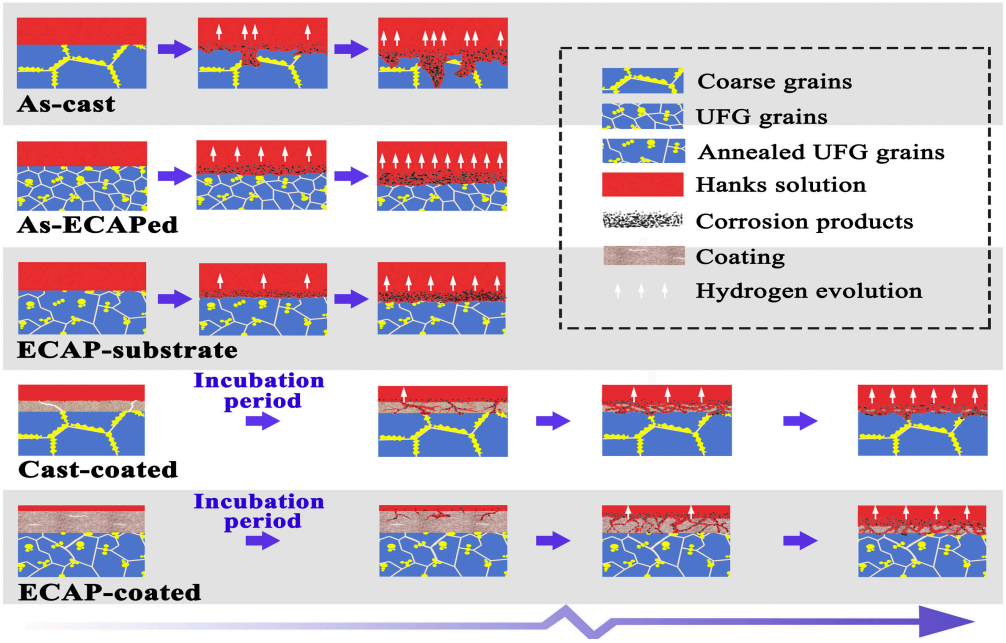

Figure 6. Schematics of corrosion degradation process and the corresponding microstructure alteration in all samples [98]. Reprinted with permission from ref. [98]. Copyright 2022 Elsevier.

6.3. Organic/Polymer Coating

Organic coatings can directly block the corrosion of harmful particles on the substrate and can prevent electrochemical cathodic reactions, thus preventing the formation of corrosive primary cells. Meanwhile, as the organic coating is insulating, the organic coating can prevent the dissolution of metal cations and inhibit the discharge, so that the substrate has better corrosion resistance. At present, organic coatings are primarily composed of polycaprolactone coatings, silane coatings, and chitosan coatings. For example, Zheng et al. evaluated [101] a metal−organic framework (MOF)−incorporated polycaprolactone film for enhanced corrosion resistance of a Mg alloy. The results showed that after the PCL coating was added, the corrosion current of the alloy was greatly reduced from 8.50×10^{-7} to 9.66×10^{-10} A/cm^2 and had a higher solution resistance. This is mainly due to the fact that the PCL hydrophobic coating provides better protection for magnesium alloys and is more resistant to the attack of electrolytes. In addition, the mixed MOF particles have good compatibility with the PCL chain, which enhances the compactness of the coating via hydrogen bonding. Thus, the composite coating has better corrosion resistance.

The silane coating on the magnesium alloy surface prevents the electrolyte from penetrating the layer and releasing corrosion products. When the silane conversion film was formed on the metal surface, it hindered the corrosion of H_2O, O_2, and the electrolyte solution in the working environment, causing the metal materials to obtain excellent corrosion resistance. For example, AhadiParsa et al. [102] assessed the bio−corrosion of a hydroxyapatite−coated AZ31 Mg alloy pre−treated with vinyl tri−ethoxy silane in SBF. The results indicated that both the hydrolysis and immersion times of pre−treatment with the silane coating markedly affect the anti−corrosion performance of the Mg substrate. Regarding the Mg alloy, which was immersed in 1 h hydrolyzed VTES for 60 s, the corrosion current density was reduced from 36.1 to a minimum of 2.1 μA/cm^2. This is because the silane coating has a better film−forming property, and the fine particles are uniformly covered on the surface of the substrate, forming a uniform film with the highest density and least defects. Moreover, by applying the HA coating on the surface of the silane−treated Mg substrate, the corrosion current was reduced to 0.9 μA/cm^2. This was the result of the presence of the silane coating as an intermediate layer, which effectively improved the anti−corrosion resistance. Additionally, Guo et al. [103] analyzed the bio−degradability and osteogenic activity of a guided bone−regeneration membrane

based on a chitosan−coated magnesium alloy (CS−Mg). The results showed that CS−Mg was degraded by hydrolysis and that its degradation proceeded slowly during the early immersion stages. This is because the chitosan coating is tightly wrapped on the surface of the Mg alloy, which reduces the porosity of the coating and avoids direct contact between the Mg alloy and the medium. Thus, the chitosan coating decreased the degradation of the Mg alloy. Additionally, a chitosan−coated−Mg alloy was used as a biodegradable barrier membrane in guided bone regeneration. Pozzo et al. [104] demonstrated the influence of the crosslinking degree on the corrosion protection properties of AZ31 chitosan coatings in simulated body fluids. The results indicated that the hydrogen evolution rate of 0.01 $mL \cdot cm^{-2} \cdot d^{-1}$ was achieved. This is due to the good adhesion between the chitosan coating and the NaOH−treated matrix, which reduces the porosity and thus the corrosion rate. Additionally, a crosslinking degree of up to 42% results in higher resistance of the chitosan coating ($R_{coating}$) and better anticorrosive properties.

Common polymer coatings include polylactic acid (PLA), which retards the initial degradation rate of the Mg alloy, limits the local alkalization caused by OH^- release, and retards the release of hydrogen. For example, Cifuentes et al. [105] studied the in vitro degradation of biodegradable polylactic acid/Mg composites by comparing a composite with a poly−L−lactic (PLLA) coating with another with a poly−L, D−lactic (PLDA) coating. The results showed that PLDA was more effective at reducing the degradation rate of Mg than PLLA. This was due to the increased hydrolysis of amorphous domains in the PLDA−cr/Mg in comparison to that of PLDA/Mg, which formed fast paths for the water to diffuse faster into the core of the samples. In contrast, the decrease in corrosion resistance of bioresorbable poly−lactic acid/Mg composites for orthopedic applications in simulated body fluid was assessed by Ali [106]. The results showed that degradation was accompanied by fiber−corrosion of α−Mg. Due to the expansion of $Mg(OH)_2$ in the corrosion process, PLA formed radial cracks in the corroded fiber, and the degradation behavior was reduced. The radial cracks in the PLA facilitated the penetration of water into the interface, which led to pitting corrosion of the fibers and fast degradation. Therefore, further surface modification of Mg fiber to delay degradation is the key to developing Mg/PLA composites for biomedical applications.

6.4. Complex Coatings

Compared with the above single coatings, two or more composite coatings could further seal the distribution of pores to form a more stable protective layer. Therefore, its degradation behavior could better meet the requirements of human implantation. For instance, Zhang et al. [107] studied the corrosion behavior of a polycaprolactone/HA composite coating on bioresorbable Mg alloys in Hanks' solution. The results indicated that the uncoated AZ31 alloy had a corrosion rate of 160 mm/y, while the AZ31 with PCL/HA coatings exhibited the smallest corrosion rate (6.9 mm/y), which was nearly 23 times lower than that of AZ31. This is because the presence of HA crystals in the PCL coating helps to enhance biomineralization and form Ca−P deposits on the surface. In addition, HA and PCL improved surface chemical compatibility and achieved chemical bonding. Moreover, the micro−nano spaces between the HA crystals constructed a rough surface for the penetration of PCL and formed a mechanical lock. Rahman et al. [108] investigated the degradation behaviors of a polymer/ceramic hybrid coating on a Mg−Zn−Ca alloy in simulated body fluid. Electrochemical tests revealed that the corrosion rate of the PCL/HA coating was 6.63×10^{-3} mm/y, which was greatly reduced by approximately 10 times and 900 times compared to the HA and un−treated Mg−Zn−Ca alloys, respectively. This is primarily because the HA membrane acts as a barrier layer to prevent the aqueous solution from penetrating the metal surface. Moreover, the nanocomposite coating of PCL/HA offered adequate and stable obstruction to fast metal dissolution, which slowed the degradation process in SBF. Moreover, the corrosion behavior of AZ31 was enhanced by the treatment of the hydroxyapatite/chitosan−metformin composite coating, which was analyzed by Li [109]. The results showed that the corrosion rate of AZ/HA/CS−MF was

1.05×10^{-3} mm/y, which was much slower than that of AZ31 (1.16×10^{-1} mm/y) and AZ31/HA (1.14×10^{-2} mm/y). This is due to the large number of particle aggregates on the surface of the AZ31/HA/CS−MF coating, which are formed by the adsorption of calcium and phosphate ions in the body fluids of SBF on the coating surface during the impregnation process. Moreover, the AZ31/HA/CS−MF coating effectively blocked corrosion ions, which had potential application as a protective coating on AZ31 for orthopedic applications. Similarly, Jin et al. [110] evaluated the biocorrosion of an HA−CS/PLA hybrid coating on a micro−arc−oxidized AZ91D Mg alloy in simulated body fluid. When the concentration of PLA was 20%, the I_{corr} was the lowest at 1.13×10^{-8} A/cm^2. This is primarily due to the fact that with the increase in the PLA concentration, PLA will further penetrate the pores to achieve a complete sealing effect, thus forming a stable corrosion barrier. In addition, He et al. [111] determined that a composite Ca−P/ZnO precoating can provide better protection for a magnesium implant than a pure PCL coating in simulated body fluids. This was primarily because the Mg elements will induce the deposition of Ca−P/ZnO compounds on the surface. Moreover, the Ca−P compounds transformed into a more stable HA layer with the increase in soaking time, which helped to retard the corrosive process of simulated body fluid on the substrate. Moreover, different proportions of doping nanoparticles resulted in different porosity and porous structures, which was helpful for controlling the degradation rate of the magnesium matrix.

Furthermore, other coatings can also greatly improve corrosion resistance. For example, Kalaiyarasan et al. [112] researched the corrosion resistance of a chitosan/silica hybrid coating on AZ31 in Earle's solution, and the corrosion rate was reduced from 0.166 to 0.01 mm/y. According to the following formulae (Equations (5)–(7)), the reason was the formation of the Mg(II) Chi complex on the intermetallic β phase, which prevented the movement of ions and reduced the rate of deposition on the metal surface, thereby preventing further cathodic reactions and reducing the hydrogen gas evolution. Additionally, the coral−like morphology formed on Ch^{-3}/Si with the nanoporous structure could offer better cell adhesion and osteointegration processes.

$$Mg + 2H_2O \rightarrow Mg(OH)_2 + H_2 \quad (5)$$

$$Chi - NH_2 + H_2O \rightarrow Chi - NH_3{}^+ + OH^- \quad (6)$$

$$Mg(OH)_2 + Chi - NH_3{}^+ \rightarrow Mg(II) - Chi - NH_2 + H_2O + H^+ \quad (7)$$

Furthermore, Gao et al. [113] studied the corrosion resistance of a chitosan/heparinized graphene oxide (Chi/HGO) multilayer coating on Mg alloys in Hanks' simulated body fluid. With the Chi/HGO coating, the corrosion potential increased to −1.376 V and the corrosion current density decreased from 8.863×10^{-5} to 7.483×10^{-7} A/cm^2. Firstly, the amino group on chitosan could promote the binding of the anion and reduce the surface positivity and prevent the further adsorption of anions, increasing the corrosion resistance. Secondly, HGO with negative charges can inhibit anionic erosion, and the Chi/HGO multilayer coating was very dense, compact, and much thicker than the monolayer chitosan film. Thus, it could provide the sample with excellent protection for a long time. On this basis, Bahatibieke et al. [114] studied the degradation behavior of anodic oxidation (AO)−silane (SA)−chitosan (CS)−coated Mg−4.0Zn−0.8Sr alloys for bone applications. The results indicated that the AO−SA−CS coating reduced the average corrosion rate of Mg alloys from 2.069 to 0.708 g·m^{-2}·d^{-1}. This was because the SA coating was hydrophobic, which can block contact between the corrosion solution and the coating sample. Moreover, the thickness of the CS coating was relatively large and can effectively prevent further contact with the corrosive environment. Moreover, after the magnesium alloy prepared by the AO−SA−CS coating was implanted into the femur of rats, the bone tissue of the rats recovered well and the kidney tissue was normal, showing good biocompatibility. Moreover, Dong et al. [115] researched the corrosion properties of a dual, self−healing, inorganic−organic hybrid coating on biomedical Mg in Hanks' balanced salt solution. The results revealed that the DCPD/H_xPh_y9 coating had the lowest I_{corr} value. The results

showed that the increase in pH of the Mg corrosion by−product and the enrichment of Mg^{2+} were double stimulants for the self−healing of the coating. Furthermore, the apatite and Mg−H_xPh_y compounds were formed as corrosion−resistant products to eliminate the local corrosion.

7. Summary and Future Prospective

Acting as a new generation of biodegradable materials (BMs), Mg alloys have great potential applications in bone repair/fixation, blood vessel stents, and oral scaffolds. In accordance with previous research results, the corrosion rate statistics of medical magnesium alloys in different processes were listed in Figure 7. It can be directly selected for research according to the degradation requirements of medical implants. However, medical Mg alloys still face many challenges in the following aspects:

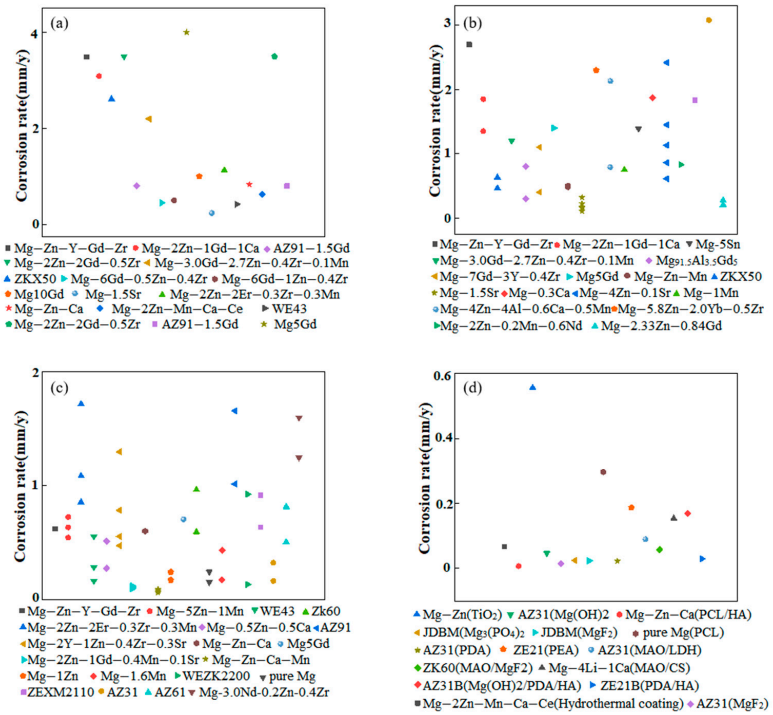

Figure 7. Corrosion performance images of magnesium alloys under different processes. (**a**) As−cast: Mg−Zn−Y−Gd−Zr [60]; Mg−2Zn−1Gd−1Ca [63]; ZKX50 [66]; Mg−2Zn−2Gd−0.5Zr, AZ91−1.5Gd, Mg−3.0Gd−2.7Zn−0.4Zr−0.1Mn, Mg−6Gd−0.5Zn−0.4Zr, Mg−6Gd−1Zn−0.4Zr, Mg5Gd, Mg10Gd [67]; Mg−1.5Sr [69]; Mg−2Zn−2Er−0.3Zr−0.3Mn [76]; WE43 [77]; Mg−Zn−Ca [83]; Mg−2Zn−Mn−Ca−Ce [98]; Mg−2Zn−2Gd−0.5Zr [116]; AZ91−1.5Gd [117]. (**b**) Heat treatment: Mg−2Zn−0.2Mn−0.6Nd, Mg−2Zn−0.2Mn−1.2Nd, Mg−2Zn−0.2Mn−1.8Nd [18]; Mg−Zn−Y−Gd−Zr [60]; Mg−2Zn−1Gd−1Ca [63]; ZKX50 [66]; Mg−3.0Gd−2.7Zn−0.4Zr−0.1Mn, $Mg_{91.5}Al_{3.5}Gd_5$, Mg−7Gd−3Y−0.4Zr, Mg5Gd [67]; Mg−Zn−Mn [68]; Mg−1.5Sr [69]; Mg−5.8Zn−2.0Yb−0.5Zr [73]; Mg−4Zn−4Al−0.6Ca−0.5Mn [118]; Mg−1Mn, Mg−5Sn, Mg−0.3Ca [119]; Mg−4Zn−0.1Sr [120]; Mg−2.33Zn−0.84Gd [121]. (**c**) Plastic deformation: Mg−Zn−Y−Gd−Zr [60]; Mg5Gd [67]; Mg−5Zn−1Mn [75]; Mg−2Zn−2Er−0.3Zr−0.3Mn [76]; WE43 [77]; Mg−0.5Zn−0.5Ca [78]; Mg−2Y−1Zn−0.4Zr−0.3Sr [80]; Mg−2Zn−1Gd−0.4Mn−0.1Sr [81]; Mg−Zn−Ca [83]; Mg−Zn−Ca−Mn [85]; Mg−1Zn [122]; ZK60, pure Mg, Mg−1.6Mn, AZ91, WEZK2200, ZEXM2110, AZ31, AZ61, Mg−3.0Nd−0.2Zn−0.4Zr [123]. (**d**) Surface modification: Mg−2Zn−Mn−Ca−Ce(Hydrothermal coating) [98]; Mg−Zn−Ca(PCL/HA) [108]; Mg−Zn(TiO_2), AZ31($Mg(OH)_2$, AZ31(MgF_2), JDBM($Mg3(PO_4)_2$), JDBM(MgF_2), pure Mg(PCL), AZ31(PDA), AZ31(MAO/LDH), Mg−4Li−1Ca(MAO/CS), AZ31B($Mg(OH)_2$/PDA/HA), ZE21B(PDA/HA), ZK60(MAO/MgF_2), ZE21(PEA) [124]. This figure is reproduced based on [18,60,63,66–69,73,75–78,80,81,83,85,98,108,116–124].

It was necessary to establish the multiple elements' selection rules consistent with the biodegradation system, so as to achieve an effective combination of common alloy elements and rare−earth elements and essentially improve the corrosion behavior and mechanical behavior of the alloy itself.

The complex environment in the human body was subject to the synergistic effect of alternating loads and corrosive media. It is necessary to achieve a long−term excellent performance of implant materials at specific sites through comprehensive and accurate in vitro and in vivo tests to meet the diversified functional requirements of biological implants.

Although Mg^{2+} could be absorbed and metabolized in the human body, it is necessary to change the release rate of magnesium ions to balance the excretion rate of magnesium in the human body.

Until now, single−process measures have shown obvious limitations and could not meet the complex requirements in vivo. It was necessary to explore the synergy effect of large plastic deformation and multiple composite coatings. However, the current combination method was not mature and still needs further experiments to verify.

Author Contributions: Conceptualization: W.L., Y.L., M.Z. and Y.Z.; methodology, W.L., L.C., Y.L. and Y.Z.; formal analysis, W.L., Y.L., Y.T. and Y.Z.; resources, Y.L. and M.Z.; data curation: Y.T., Y.Z. and M.Z.; validation, Y.Z., Y.T., Y.L. and L.C.; writing—original draft preparation: W.L., Y.L., Y.T. and L.C. All authors have read and agreed to the published version of the manuscript.

Funding: The research was supported by the Central Government Guided Local Science and Technology Development Project (226Z1004G), Science and Technology Program of Hebei (E2020209153, E2022209059), Science and Technology Project of Tangshan (20130205b).

Data Availability Statement: Not applicable.

Conflicts of Interest: The authors declare no conflict of interest.

References

1. Pradeep, N.B.; Rajath-Hegde, M.M.; Manjunath-Patel, G.C.; Giasin, K.; Pimenov, D.Y.; Wojciechowski, S. Synthesis and characterization of mechanically alloyed nanostructured *ternary* titanium based alloy for bio-medical applications. *J. Mater. Res. Technol.* **2022**, *16*, 88–101. [CrossRef]
2. Xing, F.; Li, S.; Yin, D.D.; Xie, J.C.; Rommens, P.M.; Xiang, Z.; Liu, M.; Ritz, U. Recent progress in Mg-based alloys as a novel bioabsorbable biomaterials for orthopedic applications. *J. Magnes. Alloys* **2022**, *10*, 1428–1456. [CrossRef]
3. Tipan, N.; Pandey, A.; Mishra, P. Selection and preparation strategies of Mg-alloys and other biodegradable materials for orthopaedic applications: A review. *Mater. Today. Commun.* **2022**, *31*, 103658. [CrossRef]
4. Afifi, M.; Mehrez, E.E.; Shabbir, M.; Noweir, A.A.; Wageh, S.; Abu-Saied, M.A.; El-Morsy, M.A.; Salem, W.M.; Mostafa, M.S.; Salem, S.R.; et al. Chemical stability, morphological behavior of Mg/Sr-hydroxyapatite@chitosan biocomposites for medical applications. *J. Mater. Res. Technol.* **2022**, *18*, 681–692. [CrossRef]
5. Bairagi, D.; Mandal, S. A comprehensive review on biocompatible Mg-based alloys as temporary orthopaedic implants: Current status, challenges, and future prospects. *J. Magnes. Alloys* **2022**, *10*, 627–669. [CrossRef]
6. Arora, G.S.; Sathish, R.U.; Saxena, K.K. Critical review of Mg matrix composite for bio-implants through powder metallurgy. *Mater. Today. Commun.* **2022**, *57*, 902–907.
7. Weng, W.J.; Arne, B.; Li, Y.C.; Matthew, D.; Cuie, W. A review of the physiological impact of rare earth elements and their uses in biomedical Mg alloys. *Acta Biomater.* **2021**, *130*, 80–97. [CrossRef]
8. Chen, Y.J.; Xu, Z.G.; Smith, C.; Sankar, J. Recent advances on the development of magnesium alloys for biodegradable implants. *Acta Biomater.* **2014**, *10*, 4561–4573. [CrossRef]
9. Erbel, R.; Mario, C.D.; Bartunek, J.; Bonnier, J.; Bruyne, B.D.; Eberli, F.R.; Erne, P.; Haude, M.; Heublein, B.; Horrigan, M. Temporary scaffolding of coronary arteries with bioabsorbable magnesium stents: A prospective, non-randomised multicentre trial. *Lancet* **2007**, *369*, 1869–1875. [CrossRef]
10. Cheng, P.F.; Han, P.; Zhao, C.L.; Zhang, S.X.; Wu, H.L.; Ni, J.H.; Hou, P.; Zhang, Y.Z.; Liu, J.Y.; Xu, H.D.; et al. High-purity magnesium interference screws promote fibrocartilaginous entheses regeneration in the anterior cruciate ligament reconstruction rabbit model via accumulation of BMP-2 and VEGF. *Biomaterials* **2016**, *81*, 14–26. [CrossRef]
11. Alaneme, K.K.; Kareem, S.A.; Olajide, J.L.; Sadiku, R.E.; Bodunrin, M.O. Computational biomechanical and biodegradation integrity assessment of Mg-based biomedical devices for cardiovascular and orthopedic applications: A review. *Int. J. Light-Weight. Mater. Manuf.* **2022**, *5*, 251–266. [CrossRef]

12. Krishnan, R.; Pandiaraj, S.; Muthusamy, S.; Panchal, H.; Alsoufi, M.A.; Ibrahim, A.M.M.; Elsheikh, A. Biodegradable magnesium metal matrix composites for biomedical implants: Synthesis, mechanical performance, and corrosion behavior—A Re-view. *J. Mater. Res. Technol.* **2022**, *20*, 650–670. [CrossRef]
13. Byun, S.H.; Lim, H.K.; Cheon, K.H.; Lee, S.M.; Kim, H.E.; Lee, J.H. Biodegradable magnesium alloy (WE43) in bone-fixation plate and screw. *J. Biomed. Mater. Res.* **2020**, *108*, 2505–2512. [CrossRef] [PubMed]
14. Tie, D.; Liu, H.N.; Guan, R.G.; Patricia, H.T.; Liu, Y.L.; Wang, Y.; Hort, N. In vivo assessment of biodegradable magnesium alloy ureteral stents in a pig model. *Acta Biomater.* **2020**, *116*, 415–425. [CrossRef] [PubMed]
15. Elkamel, R.S.; Fekry, A.M.; Ghoneim, A.A. Electrochemical corrosion behaviour of AZ91E magnesium alloy by means of various nanocoatings in aqueous peritoneal solution: In vitro and in vivo studies. *J. Mater. Res. Technol.* **2022**, *17*, 828–839. [CrossRef]
16. Zhang, Y.; Li, J.X.; Li, J.Y. Effects of calcium addition on phase characteristics and corrosion behaviors of Mg-2Zn-0.2Mn-xCa in simulated body fluid. *J. Alloys Compd.* **2017**, *728*, 37–46. [CrossRef]
17. Zhang, Y.; Li, J.X.; Li, J.Y. Microstructure, mechanical properties, corrosion behavior and film formation mechanism of Mg-Zn-Mn-xNd in Kokubo's solution. *J. Alloys Compd.* **2018**, *730*, 458–470. [CrossRef]
18. Zhang, Y.; Li, J.Y.; LIAW, P.K.; Xu, Y.Z.; Lai, H.Y. Effects of heat treatment on the mechanical properties and corrosion behaviour of the Mg-2Zn-0.2Mn-xNd alloys. *J. Alloys Compd.* **2018**, *769*, 552–565. [CrossRef]
19. Cai, C.H.; Song, R.B.; Wen, E.D.; Wang, Y.J.; Li, J.Y. Effect of microstructure evolution on tensile fracture behavior of Mg-2Zn-1Nd-0.6Zr alloy for biomedical applications. *Mater. Des.* **2019**, *182*, 108038. [CrossRef]
20. Li, J.X.; Zhang, Y.; Li, J.Y.; Xie, J.X. Effect of trace HA on microstructure, mechanical properties and corrosion behavior of Mg-2Zn-0. *5Sr alloy. J. Mater. Sci. Technol.* **2017**, *34*, 299–310. [CrossRef]
21. Zhang, Y.; Li, J.Y.; Liu, Y.; Chen, L.S. Microstructure characteristics, film layer rupture mechanism and corrosion behavior of hot-rolled Mg-2Zn-0. *2Mn-xNd. Mater. Charact.* **2020**, *165*, 110368. [CrossRef]
22. Liu, Y.; Zhang, Y.; Zheng, R.N.; Zheng, Y.Q.; Chen, L.S. Microstructure characteristics, degradation behaviors and film formation mechanism of Zn-1Mg-0.25Nd-xSn in the Kokubo's electrolyte. *Mater. Charact.* **2021**, *174*, 111034. [CrossRef]
23. Cai, C.H.; Alves, M.M.; Song, R.B.; Wang, Y.J.; Li, J.Y.; Montemor, M.F. Non-destructive corrosion study on a magnesium alloy with mechanical properties tailored for biodegradable cardiovascular stent applications. *J. Mater. Sci. Technol.* **2021**, *66*, 128–138. [CrossRef]
24. Woo, S.K.; Suh, B.C.; Kim, H.S.; Yim, C.D. Effect of processing history on corrosion behaviours of high purity Mg. *Corros. Sci.* **2021**, *184*, 109357. [CrossRef]
25. Gao, Y.M.; Wang, L.Z.; Li, L.H.; Gu, X.N.; Zhang, K.; Xia, J.; Fan, Y.B. Effect of stress on corrosion of high-purity magnesium in vitro and in vivo. *Acta Biomater.* **2019**, *83*, 477–486. [CrossRef] [PubMed]
26. Ma, M.Y.; Pokharel, D.B.; Dong, J.H.; Wu, L.P.; Zhao, R.Y.; Zhu, Y.; Hou, J.R.; Xie, J.Y.; Sui, S.H.; Wang, C.G.; et al. In vivo corrosion behavior of pure magnesium in femur bone of rabbit. *J. Alloys Compd.* **2020**, *848*, 156506. [CrossRef]
27. Yu, Y.Q.; Lu, H.; Sun, J. Long-term in vivo evolution of high-purity Mg screw degradation-Local and systemic effects of Mg degradation products. *Acta Biomater.* **2018**, *71*, 215–224. [CrossRef]
28. Chen, B.; Wang, D.X.; Zhang, L.; Geng, G.H.; Yan, Z.J.; Eckert, J. Correlation between the crystallized structure of Mg67Zn28Ca5 amorphous alloy and the corrosion behavior in simulated body fluid. *J. Non-Cryst. Solids* **2021**, *553*, 120473. [CrossRef]
29. Wang, C.M.; Yang, S.; Yang, Y.W.; Yang, Y.W.; Zeng, D.; Liang, X.W.; Peng, S.P.; Shuai, C.J. Amorphous magnesium alloy with high corrosion resistance fabricated by laser powder bed fusion. *J. Alloys Compd.* **2022**, *897*, 163247. [CrossRef]
30. Zai, W.; Man, H.C.; Su, Y.C.; Li, G.Y.; Lian, J.S. Impact of microalloying element Ga on the glass-forming ability (GFA), mechanical properties and corrosion behavior of Mg-Zn-Ca bulk metallic glass. *Mater. Chem. Phys.* **2020**, *255*, 123555. [CrossRef]
31. Li, K.; Li, B.H.; Du, P.; Xiang, T.; Yang, X.X.; Xie, G.Q. Effect of powder size on strength and corrosion behavior of Mg66Zn30Ca4 bulk metallic glass. *J. Alloys Compd.* **2022**, *897*, 163219. [CrossRef]
32. Makkar, P.; Sarkar, S.K.; Padalhin, A.R.; Moon, B.G.; Lee, Y.S.; Lee, B.E. In vitro and in vivo assessment of biomedical Mg–Ca alloys for bone implant applications. *J. Appl. Biomater. Funct. Mater.* **2018**, *16*, 126–136. [CrossRef] [PubMed]
33. Chen, K.; Zhao, Y.; Liu, C.L.; Li, Q.; Bai, Y.J.; Li, P.; Wang, C.; Gu, X.N.; Fan, Y.B. Novel Mg-Ca-La alloys for guided bone regeneration: Mechanical performance, stress corrosion behavior and biocompatibility. *Mater. Today. Commun.* **2022**, *32*, 103949. [CrossRef]
34. Hu, Y.P.; Guo, X.; Qiao, Y.; Wang, X.Y.; Lin, Q.C. Preparation of medical Mg–Zn alloys and the effect of different zinc con-tents on the alloy. *J. Mater. Sci. Mater. M* **2022**, *33*, 9. [CrossRef] [PubMed]
35. Abdel-Gawad, S.A.; Shoeib, M.A. Corrosion studies and microstructure of Mg-Zn-Ca alloys for biomedical applications. *Surf. Interfaces* **2019**, *14*, 108–116. [CrossRef]
36. Pan, H.; Pang, K.; Cui, F.Z.; Ge, F.; Man, C.; Wang, X.; Cui, Z.Y. Effect of alloyed Sr on the microstructure and corrosion behavior of biodegradable Mg-Zn-Mn alloy in Hanks' solution. *Corros. Sci.* **2019**, *157*, 420–437. [CrossRef]
37. Wen, Y.F.; Liu, Q.S.; Wang, J.F.; Yang, Q.M.; Zhao, W.K.; Qiao, B.; Li, Y.L.; Jiang, D.M. Improving in vitro and in vivo corrosion resistance and biocompatibility of Mg-1Zn-1Sn alloys by microalloying with Sr. *Bioact. Mater.* **2021**, *6*, 4654–4669. [CrossRef]
38. Song, J.; Gao, Y.H.; Liu, C.M.; Chen, Z.Y. The effect of Sr addition on the microstructure and corrosion behaviour of a Mg-Zn-Ca alloy. *Surf. Coat. Technol.* **2022**, *437*, 128328. [CrossRef]
39. Cho, D.H.; Avey, H.; Nam, K.H.; Dean, D.; Luo, A.A. In vitro and in vivo assessment of squeeze-cast Mg-Zn-Ca-Mn alloys for biomedical applications. *Acta Biomater.* **2022**, *150*, 442–455. [CrossRef]

40. Li, D.; Zhang, D.C.; Yuan, Q.; Liu, L.H.; Li, H.; Xiong, L.; Guo, X.N.; Yan, Y.; Yu, K.; Dai, Y.L.; et al. In vitro and in vivo assessment of the effect of biodegradable magnesium alloys on osteogenesis. *Acta Biomater.* **2022**, *141*, 454–465. [CrossRef]
41. Zhang, Y.P.; Huang, Y.D.; Feyerabend, F.; Blawert, C.; Gan, W.M.; Maawad, E.; You, S.H.; Gavras, S.; Scharnagl, N.; Bode, J.; et al. Influence of the amount of intermetallics on the degradation of Mg-Nd alloys under physiological conditions. *Acta Biomater.* **2021**, *121*, 695–712. [CrossRef] [PubMed]
42. Wang, C.; Wang, J.F.; Xu, C.; Wang, L.G.; Zhu, S.J.; Guan, S.K. Anodic Role of Mg12Nd in the Micro-Galvanic Corrosion of Binary Mg-Nd Alloys. SSRN 2022. Available online: https://ssrn.com/abstract=4172876 (accessed on 24 November 2022).
43. Wang, C.M.; Zeng, L.M.; Zhang, W.L.; Tang, F.Q.; Ding, W.C.; Xiao, S.F.; Liang, T.X. Enhanced mechanical properties and corrosion resistance of rolled Mg-1.5Sn-0.5Ca alloy by Ce microalloying. *Mater. Charact.* **2021**, *179*, 111325. [CrossRef]
44. Wang, H.J.; Kumazawa, T.; Zhang, Y.; Wang, H.W.; Ju, D.Y. In vivo degradation behaviour and bone response of a new Mg-rare earth alloy immobilized in a rat femoral model. *Mater. Today Commun.* **2021**, *26*, 101727. [CrossRef]
45. Kania, A.; Nowosielski, R.; Agnieszka, G.M.; Babilas, R. Mechanical and Corrosion Properties of Mg-Based Alloys with Gd Addition. *Materials* **2019**, *12*, 1775. [CrossRef]
46. Cheng, X.L.; Qu, Y.; Kang, C.Y.; Kang, M.Y.; Dong, R.P.; Zhao, J.W. Development of new medical Mg-Zn-Ca-Y alloy and in-vitro and in-vivo evaluations of its biological characteristics. *Mater. Today Commun.* **2021**, *26*, 102002. [CrossRef]
47. Li, H.; Wen, J.B.; He, J.G.; Shi, H.N.; Liu, Y. Effects of Dy addition on the mechanical and degradation properties of Mg-2Zn-0.5Zr alloy. *Adv. Eng. Mater.* **2020**, *22*, 1901360. [CrossRef]
48. Azzeddine, H.; Hanna, A.; Dakhouche, A.; Rabahi, L.; Scharnagl, N.; Dopita, N.; Brisset, F.; Helbert, A.L.; Baudin, T. Impact of rare-earth elements on the corrosion performance of binary magnesium alloys. *J. Alloys Compd.* **2020**, *829*, 154569. [CrossRef]
49. Dvorský, D.; Kubásek, J.; Voňavková, I.; Vojtěch, D. Structure, mechanical and corrosion properties of extruded Mg-Nd-Zn, Mg-Y-Zn and Mg-Y-Nd alloys. *Mater. Sci. Technol.* **2019**, *35*, 520–529. [CrossRef]
50. Prasad, A.; Chiu, Y.L.; Jones, I.P.; Singh, S.S.; Gosvami, N.N.; Jain, J. Role of La addition for enhancing the corrosion resistance of Mg-Dy alloy. *Corros. Eng. Sci. Technol.* **2021**, *56*, 575–583. [CrossRef]
51. Lotfpour, M.; Dehghanian, C.; Emamy, M.; Bahmani, A.; Malekan, M.; Saadati, A.; Taghizadeh, M.; Shokouhimehr, M. In-vitro corrosion behavior of the cast and extruded biodegradable Mg-Zn-Cu alloys in simulated body fluid (SBF). *J. Magnes. Alloys* **2021**, *9*, 2078–2096. [CrossRef]
52. Qiao, M.L.; Sha, J.C.; Yin, S.Q.; Liu, W.H.; Zhao, Z.; Cui, J.Z.; Zhang, Z.Q. Effect of trace copper on the microstructure, corrosion behavior and biological properties of biodegradable Mg-2Zn-1Gd-0.5Zr alloy. *J. Mater. Res. Technol.* **2022**, *18*, 1607–1622. [CrossRef]
53. Liu, Z.D.; Feyerabend, F.; Bohlen, J.; Regine, W.R.; Letzig, D. Mechanical properties and degradation behavior of binary magnesium-silver alloy sheets. *J. Phys. Chem. Solids* **2019**, *133*, 142–150. [CrossRef]
54. Ma, Y.Z.; Wang, D.X.; Li, H.X.; Yang, C.L.; Yuan, F.S.; Zhang, J.S. Microstructure, mechanical properties and corrosion behavior of quaternary Mg-1Zn-0.2Ca-xAg alloy wires applied as degradable anastomotic nails. *Trans. Nonferrous Met. Soc. China* **2021**, *31*, 111–124. [CrossRef]
55. Li, Y.; Li, T.C.; Wang, Q.L.; Zou, Y. Effects of Li on Microstructures and Corrosion Behaviors of Mg-Li-Al Alloys. *Magnes. Technol.* **2019**, *20*, 127–134.
56. Xia, D.D.; Liu, Y.; Wang, S.Y.; Zeng, R.C.; Liu, Y.S.; Zheng, Y.F.; Zhou, Y.S. In vitro and in vivo investigation on biodegradable Mg-Li-Ca alloys for bone implant application. *Sci. China Mater.* **2019**, *62*, 256–272. [CrossRef]
57. Baek, S.M.; Kim, J.K.; Min, D.W.; Park, S.S. Remarkably slow corrosion rate of high-purity Mg microalloyed with 0.05wt% Sc. *J. Magnes. Alloys* **2022**, *in press*. [CrossRef]
58. He, Y.Q.; Wang, R.C.; Yang, L.Z.; Yang, L.Y.; Liu, H.C.; Peng, C.Q.; Feng, Y. Influence of Sc on the microstructure, degradation behavior, biocompatibility in vitro and mechanical property of Mg-2Zn-0.2Zr alloy. *Mater. Design.* **2022**, *221*, 110863. [CrossRef]
59. Yang, L.Z.; Feng, Y.; He, Y.Q.; Yang, L.Y.; Liu, H.C.; Wang, X.F.; Peng, C.Q.; Wang, R.C. Effect of Sc/Sm microalloying on microstructural and properties of Mg-2Zn-0.3Ca biodegradable alloy. *J. Alloys Compd.* **2022**, *907*, 164533. [CrossRef]
60. Xu, Y.Z.; Li, J.Y.; Qi, M.F.; Gu, J.B.; Zhang, Y. Effect of extrusion on the microstructure and corrosion behaviors of biodegradable Mg-Zn-Y-Gd-Zr alloy. *J. Mater. Sci.* **2020**, *55*, 1231–1245. [CrossRef]
61. Zhang, X.; Zhang, K.; Wu, Z.Q. Effect of homogenization treatment on the corrosion behavior and mechanism of Mg-Y Al-loys. *J. Wuhan Univ. Technol.* **2020**, *35*, 635–652. [CrossRef]
62. Lv, T.; Jiang, Y.W.; Chen, J.Q.; Deng, B.B.; Peng, F.; Lin, X.Z.; Liu, G.H.; Li, C.Q.; Zheng, X.F.; Xiao, J.; et al. Effect of homogenization on the microstructure, biocorrosion resistance, and biological performance of as-cast Mg-4Zn-1Ca alloy. *Mater. Today Commun.* **2022**, *33*, 104135. [CrossRef]
63. Janbozorgi, M.; Taheri, K.K.; Taheri, A.K. Microstructural evolution, mechanical properties, and corrosion resistance of a heat-treated Mg alloy for the bio-medical application. *J. Magnes. Alloys* **2019**, *7*, 80–89. [CrossRef]
64. Gui, Y.W.; Li, Q.A.; Chen, J. Effect of heat treatment on corrosion behaviors of Mg-5Y-2Nd-3Sm-0.5Zr alloys. *Int. J. Electrochem. Sci.* **2019**, *14*, 1342–1357. [CrossRef]
65. Yan, X.D.; Wan, P.; Chen, L.Y.; Tan, L.L.; Xu, X.F.; Yang, K. Microstructural effects on mechanical properties and degradation behavior of Mg-Cu alloy. *Materialia* **2021**, *16*, 101089. [CrossRef]
66. Iranshahi, F.; Nasiri, M.B.; Warchomicka, F.G.; Sommitsch, C. Investigation of the degradation rate of electron beam processed and friction stir processed biocompatible ZKX50 magnesium alloy. *J. Magnes. Alloys* **2022**, *10*, 707–720. [CrossRef]

67. Cao, F.Y.; Zhang, J.; Li, K.K.; Song, G.L. Influence of heat treatment on corrosion behavior of hot rolled Mg5Gd alloys. *Trans. Nonferrous Met. Soc. China* **2021**, *31*, 939–951. [CrossRef]
68. Jiang, D.Y.; Dai, Y.L.; Zhang, Y.; Yan, Y.; Ma, J.J.; Li, D.; Yu, K. Effects of heat treatment on microstructure, mechanical properties, corrosion resistance and cytotoxicity of ZM21 magnesium alloy as biomaterials. *J. Mater. Eng. Perform.* **2019**, *28*, 33–43. [CrossRef]
69. Dong, J.H.; Tan, L.L.; Ren, Y.B.; Yang, K. Effect of microstructure on corrosion behavior of Mg-Sr alloy in Hank's solution. *Acta Metall. Sin.* **2019**, *32*, 305–320. [CrossRef]
70. Kang, Y.Y.; Du, B.N.; Li, Y.M.; Wang, B.J.; Sheng, L.Y.; Shao, L.Q.; Zheng, Y.F.; Xi, T.F. Optimizing mechanical property and cytocompatibility of the biodegradable Mg-Zn-Y-Nd alloy by hot extrusion and heat treatment. *J. Mater. Sci. Technol.* **2019**, *35*, 6–18. [CrossRef]
71. Chelliah, N.M.; Padaikathan, P.; Kumar, R. Evaluation of electrochemical impedance and biocorrosion characteristics of as-cast and T4 heat treated AZ91 Mg-alloys in Ringer's solution. *J. Magnes. Alloys* **2019**, *7*, 134–143. [CrossRef]
72. Del Rosario Silva Campos, M.; Blawert, C.; Mendis, C.L.; Mohedanoet, M.; Zimmermann, T.; Proefrock, D.; Zheludkevich, M.L.; Kainer, K.U. Effect of heat treatment on the corrosion behavior of Mg-10Gd alloy in 0.5% NaCl solution. *Front. Mater.* **2020**, *7*, 84. [CrossRef]
73. Li, L.; Wang, T.; Hou, M.M.; Xue, P.; Lv, H.; Huang, C.J. In vitro degradation behavior and biocompatibility of Mg-5.8Zn-2.0Yb-0.5Zr alloy during aging treatment. *Mater. Lett.* **2021**, *282*, 128682. [CrossRef]
74. Pulido-González, N.; Hidalgo-Manrique, P.; García-Rodríguez, S.; Torres, J.; Rams, J. Effect of heat treatment on the mechanical and biocorrosion behaviour of two Mg-Zn-Ca alloys. *J. Magnes. Alloys* **2022**, *10*, 540–554. [CrossRef]
75. Guo, H.; Chen, J.H.; Yan, H.G.; Xia, W.J.; Su, B.; Gong, X.L.; Yu, Z.L. Effects of the rolling strain rate-induced microstructure on biocorrosion behavior of the Mg-5Zn-1Mn alloy sheet. *Mater. Res. Express* **2019**, *6*, 8. [CrossRef]
76. Zheng, Y.Q.; Zhang, Y.; Liu, Y.; Tian, Y.Q.; Zheng, X.P.; Chen, L.S. Microstructure characteristics and corrosion behaviors of Mg-2Zn-2Er-0.3Zr-0.3Mn alloy under various rolling reductions. *Metals* **2022**, *12*, 365. [CrossRef]
77. Deng, B.; Dai, Y.L.; Lin, J.G.; Zhang, D.C. Effect of rolling treatment on microstructure, mechanical properties, and corrosion properties of WE43 alloy. *Materials* **2022**, *15*, 3985. [CrossRef]
78. Wang, H.J.; Ju, D.Y.; Wang, H.W. Preparation and characterization of Mg-RE alloy sheets and formation of amorphous/crystalline composites by twin roll casting for biomedical implant application. *Metals* **2019**, *9*, 1075. [CrossRef]
79. Dargusch, M.S.; Balasubramani, N.; Yang, N.; Johnston, S.; Ali, Y.; Wang, G.; Venezuela, J.; Carluccio, J.; Lauet, C.; Allavena, R.; et al. In vivo performance of a rare earth free Mg-Zn-Ca alloy manufactured using twin roll casting for potential applications in the cranial and maxillofacial fixation devices. *Bioact. Mater.* **2022**, *12*, 85–96. [CrossRef]
80. Cao, X.; Zhang, Z.W.; Xu, C.X.; Ren, C.L.; Yang, W.F.; Zhang, J.S. Micro-galvanic corrosion behavior and mechanical properties of extruded Mg-2Y-1Zn-0.4Zr-0.3Sr alloys with different extrusion temperament immersed in simulated body fluids. *Mater. Chem. Phys.* **2021**, *271*, 124928. [CrossRef]
81. Xu, Y.Z.; Li, J.Y.; Qi, M.F.; Guo, W.H.; Deng, Y. A newly developed Mg-Zn-Gd-Mn-Sr alloy for degradable implant applications: Influence of extrusion temperature on microstructure, mechanical properties and in vitro corrosion behavior. *Mater. Charact.* **2022**, *188*, 111867. [CrossRef]
82. Shunmugasamy, V.C.; Khalid, E.; Mansoor, B. Friction stir extrusion of ultra-thin wall biodegradable magnesium alloy tubes-Microstructure and corrosion response. *Mater. Today* **2021**, *26*, 102129. [CrossRef]
83. Ly, X.; Yang, S.; Nguyen, T. Effect of equal channel angular pressing as the pretreatment on microstructure and corrosion behavior of micro-arc oxidation (MAO) composite coating on biodegradable Mg-Zn-Ca alloy. *Surf. Coat. Technol.* **2020**, *395*, 125923. [CrossRef]
84. Horky, J.; Bryła, K.; Krystian, M.; Mozdzenet, G.; Mingler, B.; Sajti, L. Improving mechanical properties of lean Mg-Zn-Ca alloy for absorbable implants via Double Equal Channel Angular Pressing (D-ECAP). *Mater. Sci. Eng. A* **2021**, *826*, 142002. [CrossRef]
85. Kavyani, M.; Ebrahimi, G.R.; Ezatpour, H.R.; Jahazi, M. Microstructure refinement, mechanical and biocorrosion properties of Mg-Zn-Ca-Mn alloy improved by a new severe plastic deformation process. *J. Magnes. Alloys* **2022**, *10*, 1640–1662. [CrossRef]
86. Liu, G.N.; Xu, J.L.; Feng, B.J.; Liu, J.H.; Qi, D.Q.; Haung, W.Z.; Yang, P.X.; Zhang, S.J. Comparison of corrosion performance of extruded and forged WE43 Mg alloy. *Materials* **2022**, *15*, 1622. [CrossRef]
87. Wu, S.X.; Wang, S.R.; Wang, G.Q.; Yu, X.C.; Liu, W.T.; Chang, Z.Q.; Wen, D.S. Microstructure, mechanical and corrosion properties of magnesium alloy bone plate treated by high-energy shot peening. *Trans. Nonferrous Met. Soc. China* **2019**, *29*, 1641–1652. [CrossRef]
88. Guo, Y.; Wang, S.R.; Liu, W.T.; Xiao, T.; Zhu, G.D.; Sun, Z.L. The effect of laser shock peening on the corrosion behavior of biocompatible magnesium alloy ZK60. *Metals* **2019**, *9*, 1237. [CrossRef]
89. Liu, H.L.; Tong, Z.P.; Zhou, W.F.; Yang, Y.; Jiao, J.F.; Ren, X.D. Improving electrochemical corrosion properties of AZ31 magnesium alloy via phosphate conversion with laser shock peening pretreatment. *J. Alloys Compd.* **2020**, *846*, 155837. [CrossRef]
90. Singh, G.; Singh, S.; Prakash, C.; Ramakrishna, S. On investigating the soda-lime shot blasting of AZ31 alloy: Effects on surface roughness, material removal rate, corrosion resistance, and bioactivity. *J. Magnes. Alloys* **2021**, *9*, 1272–1284. [CrossRef]
91. Hou, X.N.; Qin, H.F.; Gao, H.Y.; Mankoci, S.; Zhang, R.X.; Zhou, X.F.; Ren, Z.C.; Doll, G.L.; Martini, A.; Sahai, N.; et al. A systematic study of mechanical properties, corrosion behavior and biocompatibility of AZ31B Mg alloy after ultrasonic nano-crystal surface modification. *Mater. Sci. Eng. C* **2017**, *78*, 1061–1071. [CrossRef]

92. Marchenko, E.; Baigonakova, G.; Khrustalev, A.; Zhukov, I.; Vorozhtsov, A.; Chekalkin, T.; Monogenov, A.; Garin, A.; Kim, T.W.; Kang, S.B.; et al. Microstructure and biodegradation performance of Mg-4Ca-1Zn based alloys after ultrasonic treatment and doping with nanodiamonds for biomedical applications. *Mater. Chem. Phys.* **2023**, *295*, 126959. [CrossRef]
93. Long, F.; Chen, G.Q.; Zhou, M.R.; Shi, Q.Y.; Liu, Q. Simultaneous enhancement of mechanical properties and corrosion resistance of as-cast Mg-5Zn via microstructural modification by friction stir processing. *J. Magnes. Alloys* 2021, in press. [CrossRef]
94. Rokkala, U.; Bontha, S.; Ramesh, M.R.; Balla, V.K.; Srinivasan, A.; Kailas, S.V. Tailoring surface characteristics of bioabsorbable Mg-Zn-Dy alloy using friction stir processing for improved wettability and degradation behavior. *J. Mater. Res. Technol.* **2021**, *12*, 1530–1542. [CrossRef]
95. Baghdadabad, D.M.; Baghdadabad, A.R.M.; Khoei, S.M.M. Characterization of bioactive ceramic coatings synthesized by plasma electrolyte oxidation on AZ31 magnesium alloy having different Na2SiO3·9H2O concentrations. *Mater. Today Commun.* **2020**, *25*, 101642. [CrossRef]
96. Keyvani, A.; Zamani, M.; Bahamirian, M.; Nikoomanzari, E.; Fattah-alhosseini, A.; Sina, H. Role of incorporation of ZnO nanoparticles on corrosion behavior of ceramic coatings developed on AZ31 magnesium alloy by plasma electrolytic oxidation technique. *Surf. Interfaces* **2021**, *22*, 100728. [CrossRef]
97. Kashin, A.D.; Sedelnikova, M.B.; Chebodaeva, V.V.; Uvarkinet, P.V.; Luginin, N.A.; Dvilis, E.S.; Kazmina, O.V.; Sharkeev, Y.P.; Khlusov, I.A.; Miller, A.A.; et al. Diatomite-based ceramic biocoating for magnesium implants. *Ceram. Int.* **2022**, *48*, 28059–28071. [CrossRef]
98. Song, D.; Li, C.; Liang, N.N.; Yang, F.L.; Jiang, J.H.; Sun, J.P.; Wu, G.S.; Ma, A.B.; Ma, X.L. Simultaneously improving corrosion resistance and mechanical properties of a magnesium alloy via equal-channel angular pressing and post water annealing. *Mater. Des.* **2019**, *166*, 107621. [CrossRef]
99. Li, J.; He, N.; Li, J.Y.; Fu, Q.Y.; Feng, M.C.; Jin, W.H.; Li, W.; Xiao, Y.; Yu, Z.T.; Chu, P.K.; et al. A silicate-loaded MgAl LDH self-healing coating on biomedical Mg alloys for corrosion retardation and cytocompatibility enhancement. *Surf. Coat. Technol.* **2022**, *439*, 128442. [CrossRef]
100. Mashtalyar, D.V.; Nadaraia, K.V.; Plekhova, N.G.; Imshinetskiy, I.M.; Piatkova, M.A.; Pleshkova, A.I.; Kislova, S.E.; Sinebryukhov, S.L.; Gnedenkov, S.V. Antibacterial Ca/P-coatings formed on Mg alloy using plasma electrolytic oxidation and antibiotic impregnation. *Mater. Lett.* **2022**, *317*, 132099. [CrossRef]
101. Zheng, Q.Y.; Li, J.; Yuan, W.; Liu, X.M.; Tan, L.; Zheng, Y.F.; Yeung, K.W.K.; Wu, S.L. Metal-Organic Frameworks Incorporated Polycaprolactone Film for Enhanced Corrosion Resistance and Biocompatibility of Mg Alloy. *ACS Sustain. Chem. Eng.* **2019**, *7*, 18114–18124. [CrossRef]
102. AhadiParsa, M.; Mohammadloo, H.E.; Mirabedini, S.M.; Roshan, S. Bio-corrosion assessment and surface study of hydroxyapatite-coated AZ31 Mg alloy pre-treated with vinyl tri-ethoxy silane. *Mater. Chem. Phys.* **2022**, *287*, 126147. [CrossRef]
103. Guo, Y.; Yu, Y.J.; Han, L.P.; Ma, S.S.; Zhao, J.H.; Chen, H.M.; Yang, Z.K.; Zhang, F.M.; Xia, Y.; Zhou, Y.M.; et al. Biocompatibility and osteogenic activity of guided bone regeneration membrane based on chitosan-coated magnesium alloy. *Mater. Sci. Eng. C* **2019**, *100*, 226–235. [CrossRef] [PubMed]
104. Pozzo, L.D.Y.; Conceição, T.F.D.; Spinelli, A.; Scharnagl, N.; Pires, A.T.N. The influence of the crosslinking degree on the corrosion protection properties of chitosan coatings in simulated body fluid. *Prog. Org. Coat.* **2019**, *137*, 105328. [CrossRef]
105. Cifuentes, S.C.; Lieblich, M.; Saldaña, L.; González-Carrasco, J.L.; Benavente, R. In vitro degradation of biodegradable polylactic acid/Mg composites: Influence of nature and crystalline degree of the polymeric matrix. *Materialia* **2019**, *6*, 100270. [CrossRef]
106. Ali, W.; Mónica, E.R.; Kopp, A.; Gonzalez, C.; LLorca, J. Strength, corrosion resistance and cellular response of interfaces in bioresorbable poly-lactic acid/Mg fiber composites for orthopedic applications. *J. Mech. Behav. Biomed.* **2021**, *124*, 104781. [CrossRef]
107. Zhang, C.Y.; Cheng, L.; Lin, J.J.; Sun, D.W.; Zhang, J.; Liu, H.N. In vitro evaluation of degradation, cytocompatibility and antibacterial property of polycaprolactone/hydroxyapatite composite coating on bioresorbable magnesium alloy. *J. Magnes. Alloys* **2022**, *10*, 2252–2265.
108. Rahman, M.; Chowdhury, M.A.; Mia, M.S.; Ali, M.R.; Rahman, A.; Ali, M.O.; Mahmud, S. Fabrication and characterization of hybrid coating on Mg-Zn-Ca Mg alloy for enhanced corrosion and degradation resistance as medical implant. *Ceram. Int.* **2022**, *48*, 23314–23324. [CrossRef]
109. Li, H.Y.; Qin, Z.N.; Ouyang, Y.Q.; Zheng, B.; Wei, H.; Ou, J.; Shen, C. Hydroxyapatite/chitosan-metformin composite coating enhances the biocompatibility and osteogenic activity of AZ31 magnesium alloy. *J. Alloys Compd.* **2022**, *909*, 164694. [CrossRef]
110. Jin, J.; Chen, X.H.; Zhou, S.W. Biocorrosion evaluation and bonding strength of HA-CS/PLA hybrid coating on microarc oxidised AZ91D magnesium alloy. *Mater. Technol.* **2022**, *37*, 503–510. [CrossRef]
111. He, H.; Li, K.; Luo, W.; Jiao, Z.Y.; Ai, F.R.; Zhou, K.; Cao, C.L. Structure design, preparation and performance of a novel composite coating on medical magnesium-zinc alloy. *Surf. Coat. Technol.* **2022**, *443*, 128643. [CrossRef]
112. Kalaiyarasan, M.; Pugalmani, S.; Rajendran, N. Fabrication of chitosan/silica hybrid coating on AZ31 Mg alloy for orthopaedic applications. *J. Magnes. Alloys* 2022, in press. [CrossRef]
113. Gao, F.; Hu, Y.D.; Gong, Z.H.; Liu, T.; Gong, T.; Liu, S.; Zhang, C.; Quan, L.; Kaveendran, B.; Pan, C.J.; et al. Fabrication of chitosan/heparinized graphene oxide multilayer coating to improve corrosion resistance and biocompatibility of magnesium alloys. *Mater. Sci. Eng. C* **2019**, *104*, 109947. [CrossRef] [PubMed]

114. Bahatibieke, A.; Qin, H.M.; Cui, T.; Liu, Y.; Wang, Z.X. In vivo and in simulated body fluid degradation behavior and biocompatibility evaluation of anodic oxidation-silane-chitosan-coated Mg-4.0Zn-0.8Sr alloy for bone application. *Mater. Sci. Eng. C* **2021**, *120*, 111771. [CrossRef] [PubMed]
115. Dong, Q.S.; Dian, J.W.; Qian, K.; Liu, H.; Zhou, X.X.; Yao, Q.Q.; Lu, M.M.; Chu, C.L.; Xue, F.; Bai, J.; et al. Dual self-healing inorganic-organic hybrid coating on biomedical Mg. *Corros. Sci.* **2022**, *200*, 110230. [CrossRef]
116. Chen, J.X.; Tan, L.L.; Yu, X.M.; Yang, K. Effect of minor content of Gd on the mechanical and degradable properties of as-cast Mg-2Zn-xGd-0.5Zr alloys. *J. Mater. Sci. Technol.* **2019**, *35*, 503–511. [CrossRef]
117. Yin, Z.; Chen, Y.; Yan, H.; Zhou, G.H.; Wu, X.Q.; Hu, Z. Effects of the second phases on corrosion resistance of AZ91-xGd alloys treated with ultrasonic vibration. *J. Alloys Compd.* **2019**, *783*, 877–885. [CrossRef]
118. Zhang, Z.Q.; Yang, Y.X.; Li, J.A.; Zeng, R.C.; Guan, S.K. Advances in coatings on magnesium alloys for cardiovascular stents–A review. *Bioact. Mater.* **2021**, *6*, 4729–4757. [CrossRef]
119. Li, L.; Zhang, M.; Li, Y.; Zhao, J.; Qin, L.; Lai, Y.X. Corrosion and biocompatibility improvement of magnesium-based alloys as bone implant materials: A review. *Regen. Biomater.* **2017**, *4*, 129–137. [CrossRef]
120. Bahmani, A.; Lotfpour, M.; Taghizadeh, M.; Kim, W.J. Corrosion behavior of severely plastically deformed Mg and Mg alloys. *J. Magnes. Alloys* **2022**, *10*, 2607–2648. [CrossRef]
121. Kalayeh, P.M.; Malekan, M.; Bahmani, A.; Lotfpour, M.; Fatemi, S.M.; Zonoozi, S.B. Combination of severe plastic deformation and heat treatment for enhancing the corrosion resistance of a new Magnesium alloy. *J. Alloys Compd.* **2022**, *927*, 166939. [CrossRef]
122. Cao, F.Y.; Shi, Z.M.; Song, G.L.; Liu, M.; Atrens, A. Corrosion behaviour in salt spray and in 3.5% NaCl solution saturated with Mg(OH)2 of as-cast and solution heat-treated binary Mg–X alloys: X = Mn, Sn, Ca, Zn, Al, Zr, Si, Sr. *Corros. Sci.* **2013**, *76*, 60–97. [CrossRef]
123. Gong, X.L.; Chen, J.H.; Yan, H.G.; Xia, W.J.; Su, B. Effects of aging treatment and pre-deformation on stress corrosion cracking of magnesium alloy. *J. Mater. Res. Technol.* 2022, in press. [CrossRef]
124. Miao, H.W.; Huang, H.; Shi, Y.J.; Zhang, H.; Pei, J.; Yuan, G.Y. Effects of solution treatment before extrusion on the microstructure, mechanical properties and corrosion of Mg-Zn-Gd alloy in vitro. *Corros. Sci.* **2017**, *122*, 90–99. [CrossRef]